Eur. Phys. J. B **17**, 481–497 (2000)

THE EUROPEAN PHYSICAL JOURNAL B

EDP Sciences

Fibril stability in solutions of twisted β-sheet peptides: a new kind of micellization in chiral systems

I.A. Nyrkova[1,a], A.N. Semenov[1], A. Aggeli[2], and N. Boden[2]

[1] Department of Applied Mathematics, University of Leeds, Leeds LS2 9JT, UK
[2] Centre for Self-Organising Molecular Systems, University of Leeds, Leeds LS2 9JT, UK

Received 7 May 1999 and Received in final form 15 February 2000

Abstract. The problem of fibril (fibre) formation in chiral systems is explored theoretically being supported by experiments on synthetic *de novo* 11-mer peptide forming self-assembled β-sheet tapes. Experimental data unambiguously indicate that the tapes form fibrils of nearly monodisperse thickness *ca.* 8-10 nm. Fibril formation and stabilisation are attributed to inter-tape face-to-face attraction and their intrinsic twist, correspondingly. The proposed theory is capable of predicting the fibril aggregation number and its equilibrium twist in terms of molecular parameters of the primary tapes. The suggested novel mechanism of twist stabilisation of finite aggregates (fibrils) is different to the well-known stabilisation of micelles in amphiphilic systems, and it is likely to explain the formation and stability of fibrils in a wide variety of systems including proteinaceous amyloid fibres, sickle-cell hemoglobin fibres responsible for HbS anemia, corkscrew threads found in chromonics in the presence of chiral additives and native cellulose microfibrillar crystallites. The theory also makes it possible to extract the basic molecular parameters of primary tapes (inter-tape attraction energy, helical twist step, elastic moduli) from the experimental data.

PACS. 36.20.Ey Conformation – 61.46.+w Clusters, nanoparticles, and nanocrystalline materials – 87.15.-v Biomolecules: structure and physical properties

1 Introduction

Most of natural peptides are linear polymers containing L-aminoacid residues [1,2]. The peptide secondary structure (alpha-helix or beta-sheet, Figs. 1b, c) is determined by regular arrangements of hydrogen bonds as well as side-chain interactions. The same peptide sometimes can exist in different conformations: random coils, α-helices and β-sheets (see Figs. 1a, b, c) depending on solution conditions such as temperature, pH, ionic strength, solvent composition.

Experimentally, we deal with solutions of identical synthetic *de novo* peptide molecules (DN1) which, if the peptide concentration is not very low, self-assemble into long β-sheet structures (ribbon-like 'tapes', Figs. 1c, d) due to inter-molecular hydrogen-bonds and side chain attraction [3–5] (see Sect. 3 for more details). Note that individual peptides in the tape adopt stretched rod-like conformation. The rationally designed primary structure of DN1 molecules ensures that the tape structure is nearly perfect: all peptides are aligned and connected in the same way (Fig. 1c); defects like shown in Figure 1e are extremely rare. The tapes are typically very long (up to several micrometers length at high enough concentrations), Figure 2a. The ends of side groups of the peptides which form the side surfaces of the tapes can attract each other, hence a possibility of stacked β-structures (which may look like *fibrils*) – many-folded aggregates of parallel tapes, Figure 1f.

In practice thread-like fibrils stabilized by face-to-face attraction between the tapes are indeed often observed in DN1 solutions, Figure 2b. The most striking feature is that the thickness of fibrils is finite and is practically monodisperse. From the first sight, this seems unexpected as usually an attraction between molecules results in formation of infinite aggregates, *i.e.* ultimate phase separation (*e.g.* precipitation of liquid or crystalline phases in the case of small molecules, or precipitation of polymer globules in the case of macromolecules) or in formation of strongly polydisperse one-dimensional aggregates as for the case of living polymers when the monomers are capable of formation of two bonds (the primary tapes, Fig. 1c, under consideration are an example of such living polymer). Thus with face-to-face attraction between tapes, one should expect formation of very thick reams and even infinite stacks at high enough concentration, Figure 3a. However, experiments indicate that the fibril thickness is finite (Figs. 2b, c): each fibril is formed

[a] e-mail: irina@amsta.leeds.ac.uk

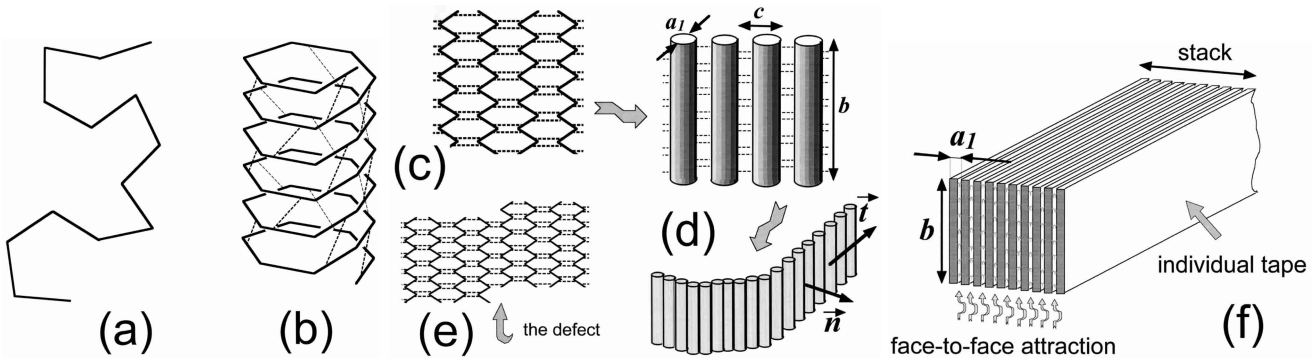

Fig. 1. Schematic representation of the classical types of secondary structures adopted by linear peptide molecules consisting of L-aminoacids: random coil (a), alpha-helix (b), beta-sheet (c). Schematic picture of an antiparallel β-sheet structure formed by self-assembled peptides (c), *i.e.* a tape (d). A defect in a beta-sheet (e), a stack of sheets (tapes) (f). Each aminoacid residue is drawn by two consequent segments in (a, b) and by one segment in (c, e). The hydrogen bonds are drawn by dotted lines. Individual tape sizes are determined by the geometry of the peptide in a rod-like conformation ($a_1 \times b \times c$), see (d, f). The primary tape trajectory can be described by the orientation of the cotangent vector **t** and by the unit vector **n** locally normal to the side surface of the tape (d).

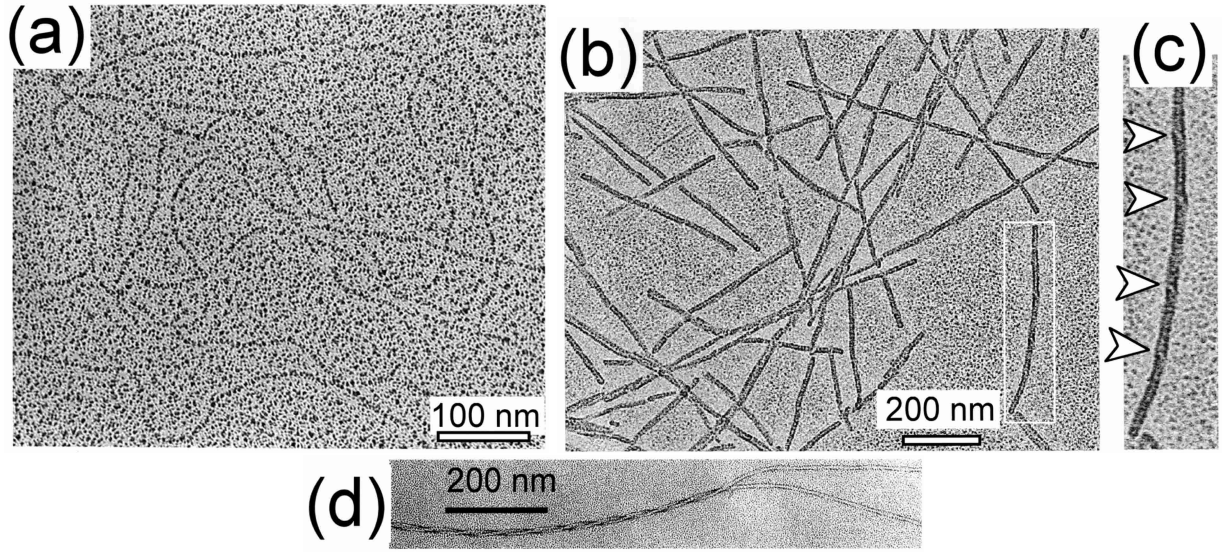

Fig. 2. Structures formed in solutions of DN1 peptide in pure water as revealed by electron microscope. The images (a) of ribbons ($c = 0.2$ mM), and (b) of fibrils ($c = 6.2$ mM) were obtained with four-month aged solutions after platinum rotary shadowing. The area surrounded with the white rectangular in (b) is shown zoomed by 200% in (c), where the positions of the characteristic crew-like patterns on the fibril are indicated with white arrows. Micrograph (d) ($c = 6.2$ mM) shows two fibrils combining into a rope-like fibre; it was obtained with a one-month aged solution after uranyl acetate negative staining.

by about a dozen of tapes assembled together. Such behavior resembles micellization in amphiphilic systems (like in surfactant solutions, Fig. 3b), involving molecules containing chemical units of at least *two different* natures (like block-copolymers). However the primary DN1 tapes are homogeneous. So, what is the reason why the thickness of the reams (fibrils) formed in DN1 solution is limited?

The explanation of this paradox is given below. All peptide molecules (both biological and synthetic like those used in our experiments) are chiral. Hence, the equilibrium structure of the primary β-sheet tapes must be naturally twisted [1,2], Figure 4a, cp. Figures 1d, f. In order to combine together and form a ream, such twisted tapes must either untwist completely (see Fig. 3a) or they should inter-twist together, Figure 4b. In the latter case their axes deviate from the straight lines (Fig. 4c). They can also partially untwist compared to the initial equilibrium structure, Figure 4a. The more tapes are combined into a ream, the stronger are these distortions of the individual tapes. Both ways of the ream formation (complete untwisting and twisting together) imply some energy cost, as the structure of tapes in the ream does not coincide with the single-tape equilibrium structure. We show below that both situations are in principle possible depending on the values of molecular parameters. However, for a particular case of a weak face-to-face attraction it is the latter situation which costs less energy, hence the tapes combine into

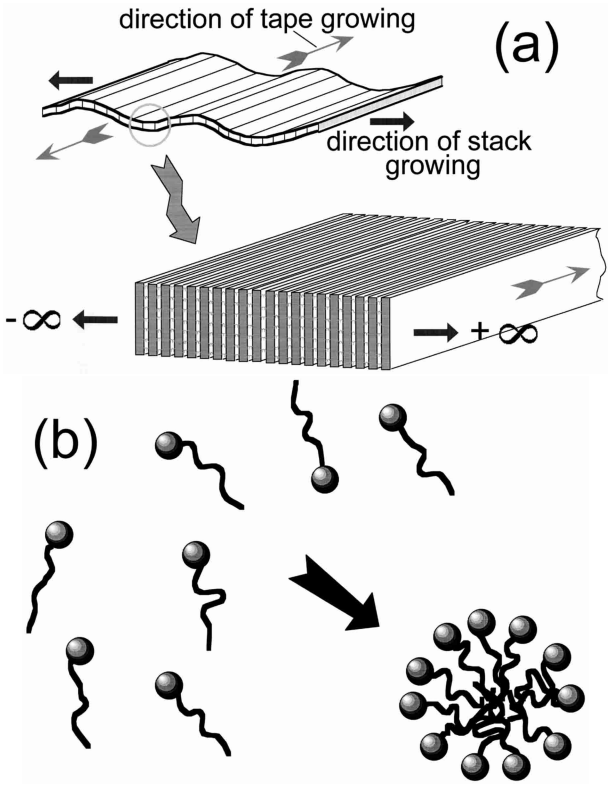

Fig. 3. (a) The most naive picture: face-to-face attraction should cause formation of an infinite stack (*i.e.* a sheet formed by parallel stacked tapes (ribbons)). (b) An example of a finite size self-assembling structure: spherical micelles are formed in solution of surfactants.

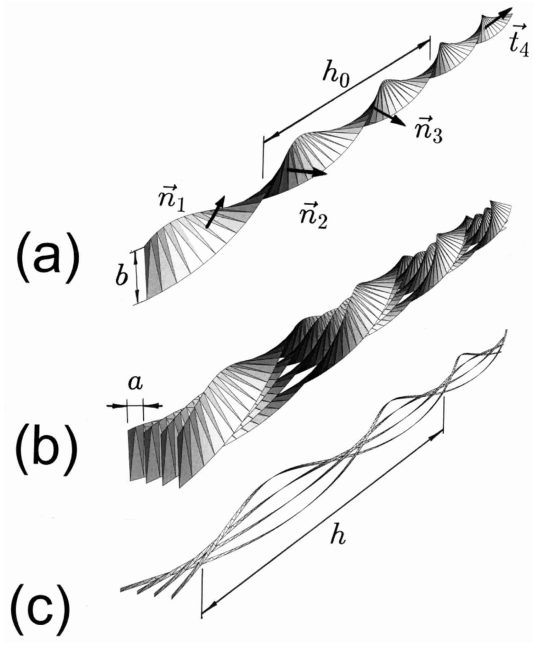

Fig. 4. Equilibrium structure of a chiral peptide beta-sheet ribbon: the central axis is straight and the ribbon is twisted around its axis with the step h_0 (a). Four ribbons combined into a stack (b) and their inter-twisted and bent axes (c). For the clarity of the illustration the ribbons are shown as infinitely thin sheets, separated by the distance a in the stack.

a *twisted* fibril. The width of the stack (the fibril thickness) is thus stabilized at some finite level when the cost of distortions of all tapes is balanced by the energy gain due to the face-to-face attraction.

Thus the fibril size is stabilized by the twisted character of the tapes. This is a unique situation when a microphase formation (precipitation into finite fibrils which is similar to micellization) takes place in a homogeneous material (uniform tapes, rather than surfactants, block-copolymers or other amphiphilic molecules). The general theoretical approach is described in the next section. The experimental results on the DN1 peptides are considered in Section 3. In Section 4 we estimate the basic microscopic characteristics of the DN1 peptide tapes using both the theory and the experimental data.

2 Theory for fibrils stabilized by twist

2.1 Model and fibril's free energy

Let us assume that each tape has a rectangular cross-section $a \times b$, $a < b$, that the opposite sides of the tape are physically the same, and that its equilibrium state is a straight helix with a step $h_0 \gg a$, Figure 4. Such special kind of a tape will be called *ribbon*, cp.with our general classification outlined in reference [5]. When two tapes (ribbons) stick together by their wider sides they gain the energy (per unit length)

$$\mathcal{E}_{\rm attr} = -\sigma b \tag{1}$$

due to surface attraction, σ is the corresponding attraction energy per unit area of contact. Simultaneously, each ribbon deviates from the equilibrium straight twisted state (Figs. 4b, c), thus increasing the elastic energy. Below we calculate the elastic energy increment.

For the sake of simplicity we assume that the ribbon contour length is fixed and that the ribbon conformation is completely determined by two unit vector fields: $\{\mathbf{t}(s), \mathbf{n}(s)\}$, where $\mathbf{t}$ is the local cotangent vector (along the ribbon axis) and $\mathbf{n}$ is the vector locally normal to the wider side (side surface) of the ribbon, Figures 1d, 4a. Here s is the distance along the ribbon axis. In the general case the elastic energy (per unit contour length) of a deformed (bent and/or twisted) ribbon can be written as $\mathcal{E}_{\rm elast} = \mathcal{E}_{\rm elast}\left(\frac{\mathrm{d}\mathbf{t}}{\mathrm{d}s}, \frac{\mathrm{d}\mathbf{n}}{\mathrm{d}s}, \mathbf{t}, \mathbf{n}\right)$. The first derivatives of the vectors $\mathbf{t}$ and $\mathbf{n}$ characterize the amplitude of the corresponding local bending/twisting in a particular direction. It is convenient to use the ribbon's own reference frame $\{\mathbf{t}(s), \mathbf{n}(s), \mathbf{m}(s)\}$, where $\mathbf{m}(s) \equiv [\mathbf{t} \times \mathbf{n}]$; then

$$\frac{\mathrm{d}\mathbf{t}}{\mathrm{d}s} \equiv (0, \nu, t_m)\,, \quad \frac{\mathrm{d}\mathbf{n}}{\mathrm{d}s} \equiv (-\nu, 0, n_m) \tag{2}$$

(we used here the fact that $\mathbf{tn} = 0$, hence $\frac{\mathrm{d}\mathbf{t}}{\mathrm{d}s}\mathbf{n} + \frac{\mathrm{d}\mathbf{n}}{\mathrm{d}s}\mathbf{t} = 0$, and also that $\mathbf{t}^2 = \mathbf{n}^2 = 1$). Here ν corresponds to bend, t_m to splay, and n_m to twist. The initial equilibrium

straight twisted conformation of a ribbon corresponds to $\nu = t_m = 0$ and $n_m = n_m^{(0)} = 2\pi/h_0 \equiv \gamma_0 = \text{const.}$, where h_0 is the twist step (the twist double period), see Figure 4a. If the deviation from the initial conformation is weak, the energy $\mathcal{E}_{\text{elast}}$ can be written as a series expansion in deformations. The main (second-order) terms of this expansion are[1]

$$\mathcal{E}_{\text{elast}} = \frac{1}{2}k_{\text{bend}}\,\nu^2 + \frac{1}{2}k_{\text{splay}}\,t_m^2 + \frac{1}{2}k_{\text{twist}}\left(n_m - n_m^{(0)}\right)^2 + \tilde{k}_1\nu t_m + \tilde{k}_2\nu n_m + \tilde{k}_3 t_m n_m. \quad (3)$$

As both sides of the ribbon are equivalent[2] the substitution $\mathbf{n}(s) \to -\mathbf{n}(s)$ (with $s \to s$, $\mathbf{t} \to \mathbf{t}$, $\mathbf{m} \to -\mathbf{m}$) must not change the energy; ν and t_m change the sign under this substitution and n_m is invariant, hence $\tilde{k}_2 = \tilde{k}_3 \equiv 0$. As both ends of the ribbon are also equivalent[3], the substitution $s \to -s$, $\mathbf{t} \to -\mathbf{t}$, $\mathbf{n} \to \mathbf{n}$, $\mathbf{m} \to -\mathbf{m}$ conserves the energy as well; now t_m changes the sign and ν and n_m are invariant, hence $\tilde{k}_1 = \tilde{k}_3 \equiv 0$[4]. Thus we have proved that the elastic energy of a twisted ribbon includes only three first terms in the expansion 3:

$$\mathcal{E}_{\text{elast}} = \frac{1}{2}k_{\text{bend}}\,\nu^2 + \frac{1}{2}k_{\text{splay}}\,t_m^2 + \frac{1}{2}k_{\text{twist}}\left(n_m - n_m^{(0)}\right)^2 \quad (4)$$

(cp. Ref. [8] where it was assumed that $k_{\text{bend}} = k_{\text{splay}}$) [5]. Note that the elastic energy formula 4 has benefitted from the natural symmetry of a ribbon, as considered at the beginning of this section[6].

Now we calculate the elastic energy of the ribbons forming a fibril of p ribbons. In the first approximation the thickness of each ribbon remains constant ($= a$), hence the vector function $\mathbf{r}_j(z)$ defining the axis of the ribbon number j ($1 \le j \le p$) in a twisted stack-like fibril (in the absolute reference frame $\{x, y, z\}$, where z is the coordinate along the fibril axis) is

$$\mathbf{r}_j = z\hat{\mathbf{z}} + \rho_j\mathbf{n}(z); \quad \mathbf{n}_j = \mathbf{n}(z) = (\cos(\gamma z), \sin(\gamma z), 0); \quad \rho_j \equiv a\left(j - \frac{p+1}{2}\right) \quad (5)$$

where $\gamma = 2\pi/h$ is the twist strength (= twist angle per unit length), $\mathbf{n}_j$ is the vector normal to side surface of ribbon j, $\hat{\mathbf{z}}$ is the unit z-coordinate vector, and p is the aggregation number (number of ribbons per fibril). The contour length element along the axis of ribbon j is

$$\mathrm{d}s_j = Q_j\,\mathrm{d}z, \quad Q_j \equiv \left(1 + \gamma^2\rho_j^2\right)^{1/2}.$$

After simple algebra we get

$$\mathbf{t}_j = \left(-\frac{\gamma\rho_j}{Q_j}\sin(\gamma z), \frac{\gamma\rho_j}{Q_j}\cos(\gamma z), \frac{1}{Q_j}\right);$$
$$\mathbf{m}_j = \left(-\frac{1}{Q_j}\sin(\gamma z), \frac{1}{Q_j}\cos(\gamma z), -\frac{\gamma\rho_j}{Q_j}\right);$$
$$\nu_j = -\frac{\gamma^2\rho_j}{Q_j^2}; \quad (t_m)_j = 0; \quad (n_m)_j = \frac{\gamma}{Q_j^2}. \quad (6)$$

Thus the elastic energy 4 of ribbon number j is:

$$\mathcal{E}_{\text{elast}}^{(j)} = \frac{1}{2}k_{\text{bend}}\frac{\gamma^4\rho_j^2}{\left(1+\gamma^2\rho_j^2\right)^2} + \frac{1}{2}k_{\text{twist}}\left(\frac{\gamma}{1+\gamma^2\rho_j^2} - \gamma_0\right)^2 \quad (7)$$

and the average elastic energy per ribbon in a fibril is

$$\bar{\mathcal{E}}_{\text{elast}} = \frac{1}{p}\sum_{j=1}^{p}\mathcal{E}_{\text{elast}}^{(j)}. \quad (8)$$

Combining equations (1, 7, 8) we get the average energy of a ribbon in the fibril formed by p ribbons:

$$\begin{aligned}\mathcal{E} &= \bar{\mathcal{E}}_{\text{elast}} + \frac{p-1}{p}\mathcal{E}_{\text{attr}} \\ &= \frac{1}{2}k_{\text{bend}}\frac{\gamma^4a^2}{p}\sum_{j=1}^{p}\frac{\left(j-(p+1)/2\right)^2}{\left(1+\gamma^2a^2\left(j-(p+1)/2\right)^2\right)^2} \\ &\quad + \frac{1}{2}k_{\text{twist}}\frac{\gamma^2}{p}\sum_{j=1}^{p}\left(\frac{1}{1+\gamma^2a^2\left(j-(p+1)/2\right)^2} - \frac{\gamma_0}{\gamma}\right)^2 \\ &\quad - \frac{p-1}{p}\sigma b. \end{aligned} \quad (9)$$

The equilibrium structure of the fibril can be obtained by minimization of the energy (9) with respect to the twisting strength γ and the aggregation number p. The fibrils are stable if the resulting net $\mathcal{E}$ is negative.

[1] Essentially the same expansion 3 was used by Marko and Siggia for description of elastic energy of B-DNA double helix, see equation (2) in reference [7].

[2] This is true for DN1 ribbon which is a double β-sheet tape, see Section 3 and Figure 5a. However, this is not the case for B-DNA structure which is not symmetric with respect to a 180° rotation around its main axis, cp. reference [7].

[3] This symmetry argument works *both* for DN1 double tape (ribbon) and for B-DNA.

[4] With similar symmetry argument it is possible to show that the only *linear* term allowed in equation (3) is const $\times n_m$. This term is included in the free energy, equation (3), in the form $-k_{\text{twist}}n_m^{(0)}n_m$.

[5] Obviously a splay deformation is very unfavourable for a ribbon with $b \gg a$: $k_{\text{splay}} \gg k_{\text{bend}}$, so that ribbons must tend to avoid any splay.

[6] The general case of a *curly tape* symmetry (see classification in ref. [5]), which applies to both B-DNA molecules [7] and single β-sheet tapes like K24 [3,4], implies the following expansion: $\mathcal{E}_{\text{elast}} = \frac{1}{2}k_{\text{bend}}\left(\nu - \nu^{(0)}\right)^2 + \frac{1}{2}k_{\text{splay}}t_m^2 + \frac{1}{2}k_{\text{twist}}\left(n_m - n_m^{(0)}\right)^2 + \tilde{k}_2\nu n_m$ (note two extra terms $k_{\text{bend}}\nu\nu^{(0)}$ and $\tilde{k}_2\nu n_m$, cp. Ref. [7])

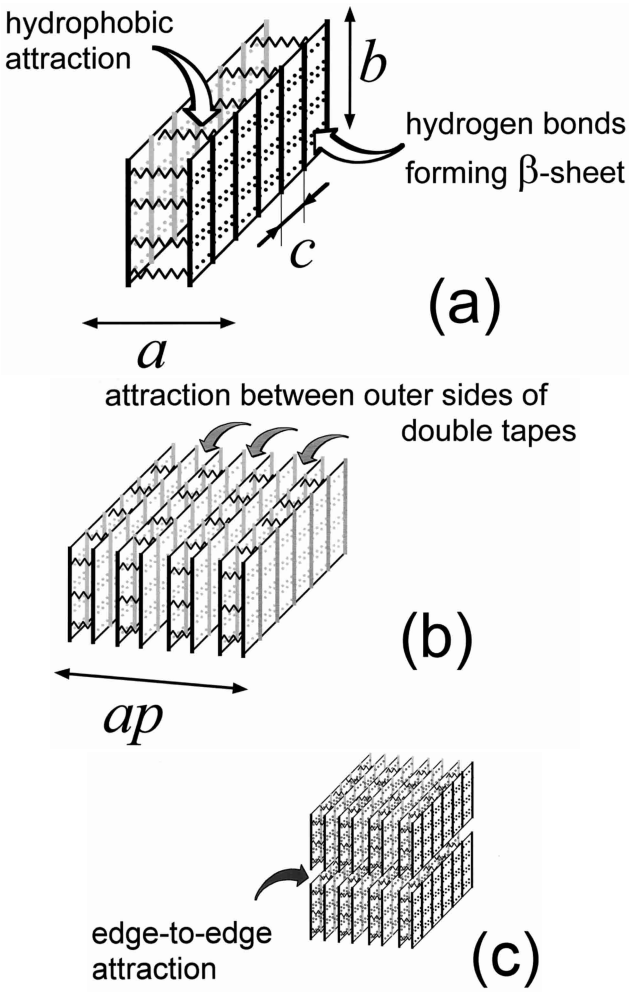

Fig. 5. Local arrangements of DN1 peptide molecules inside a ribbon (double tape) (a), inside a fibril composed of $p = 4$ double tapes (b) and inside a fibre composed of two fibrils (c). The twist is not apparent for these short fragments. The essential interactions responsible for self-assembling are indicated. Geometrical sizes for DN1 are: $a \simeq 20{-}25$ Å, $b \simeq 37$ Å, $c \simeq 4.7$ Å (see Eq. (32)).

2.2 'Many-folded' fibrils

Usually the aggregation number is rather large: $p \gg 1$. For this limit the sums in equation (9) can be approximated by the corresponding integrals which are evaluated analytically. The energy (9) can thus be rewritten as

$$\mathcal{E} \simeq k_{\rm twist}\gamma_0^2 \left\{ \frac{\beta}{4\beta_0^2}\left[\tilde{k}\left(C(\beta)-D(\beta)\right)+\left(C(\beta)+D(\beta)\right)\right] - \frac{C(\beta)}{\beta_0}+\frac{\tilde{\sigma}}{2\beta_0}\right\} + k_{\rm twist}\gamma_0^2\left(\frac{1}{2}-\frac{\tilde{\sigma}}{\gamma_0 a}\right) \tag{10}$$

with the following new parameters introduced

$$\beta_0 \equiv \frac{\gamma_0 ap}{2} \equiv \pi\frac{ap}{h_0}, \quad \beta \equiv \frac{\gamma ap}{2} \equiv \pi\frac{ap}{h}, \quad \tilde{k} \equiv \frac{k_{\rm bend}}{k_{\rm twist}}, \quad \tilde{\sigma} \equiv \frac{\sigma ab}{\gamma_0 k_{\rm twist}}, \tag{11}$$

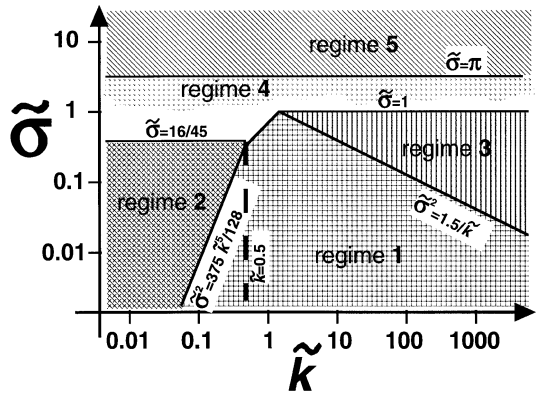

Fig. 6. The scaling diagram of regimes for solution of twisted ribbons forming fibrils in variables $\tilde{k} = k_{\rm bend}/k_{\rm twist}$, $\tilde{\sigma} = \sigma ab/(\gamma_0 k_{\rm twist})$. The twist of the fibrils is practically identical to the twist of primary ribbons, $\gamma \simeq \gamma_0$, in regime 1, equations (A.10, A.11) and in regime 2, equations (A.16, A.17). The fibrils are 'thin' and strongly untwisted, $\gamma \ll \gamma_0$, in regime 3, equations (A.21, A.22). In regime 4 (Eqs. (B.3, B.4)) wide stacks (sheets) are formed, and in regime 5 the width of the stacks tends to infinity.

$$C(\beta) \equiv \arctan(\beta), \quad D(\beta) \equiv \frac{\beta}{1+\beta^2}\cdot \tag{12}$$

The minimization of the free energy $\mathcal{E}$ with respect to γ and p is now equivalent to the minimization with respect to β and β_0. Note that $\tilde{k}$ and $\tilde{\sigma}$ are molecular constants, the last term in equation (10) is constant as well, hence we should focus on the term in curly brackets in equation (10). The values β and β_0 corresponding to the minimum are completely determined by the values of the parameters $\tilde{k}$ and $\tilde{\sigma}$ *via* the following equations:

$$\beta_0 = \beta\frac{(1+\tilde{k})C(\beta)+(1-\tilde{k})D(\beta)}{2C(\beta)-\tilde{\sigma}} \tag{13}$$

$$\beta_0 = \frac{\left[(1+\tilde{k})C(\beta)+(1-\tilde{k})D(\beta)\right]}{4C'(\beta)} + \frac{\beta\left[(1+\tilde{k})C'(\beta)+(1-\tilde{k})D'(\beta)\right]}{4C'(\beta)} \tag{14}$$

where C' and D' are the derivatives of the corresponding functions:

$$C'(\beta) \equiv \frac{1}{1+\beta^2}; \quad D'(\beta) \equiv \frac{1-\beta^2}{(1+\beta^2)^2}\cdot \tag{15}$$

In order to find the equilibrium fibril structure (for $p \gg 1$) one has to minimize the energy (10) (*i.e.* to solve the system of Eqs. (13, 14)). Below we first consider the relevant asymptotic regimes and then the general case. The corresponding scaling regimes are shown in Figure 6.

2.3 Asymptotic regimes

Equations (10, 13, 14) allow for analytical analysis of the limiting cases when the effective fibril width is small,

$\beta \ll 1$ (Appendix A), or when it is large, $\beta \gg 1$ (Appendix B).

The results for these two limiting cases are listed below. In all the cases the molecular parameters of the primary ribbons (their width a, twist γ_0, the ratio of the elastic constants $\tilde{k}$ and the effective attraction energy $\tilde{\sigma}$) are considered as known parameters, and we calculate the aggregation number p and the twist γ of the equilibrium fibril. We distinguish between three different regimes for $\beta \ll 1$ and two different regimes for $\beta \gg 1$ (five asymptotic regimes all together).

In the case of *'thin' fibrils* ($\beta \ll 1$), the free energy per ribbon (10) can be approximated as truncated series of β and minimized as explained in Appendix A. Depending on which of the terms in the series (A.2) are most important, we distinguished between three regimes of different scaling behaviors, see *regimes 1, 2 and 3* in Figure 6. The results for the parameters of the equilibrium fibril (p, γ) are:

$$pa\gamma_0 \simeq \left(\frac{12\tilde{\sigma}}{\tilde{k}}\right)^{1/3}; \quad \frac{\gamma_0-\gamma}{\gamma_0} \simeq \left(\frac{12\tilde{\sigma}}{\tilde{k}}\right)^{2/3} \frac{\tilde{k}-1/2}{6} \quad \text{in regime 1,} \quad (16)$$

$$pa\gamma_0 \simeq (90\tilde{\sigma})^{1/5}; \quad \frac{\gamma_0-\gamma}{\gamma_0} \simeq -\left(\frac{25\tilde{\sigma}^2}{768}\right)^{1/5} \quad \text{in regime 2,} \quad (17)$$

$$ap\gamma_0 \simeq \frac{4\tilde{k}\tilde{\sigma}^3}{3}; \quad \gamma \simeq \gamma_0 \frac{3}{2\tilde{k}\tilde{\sigma}^2} \quad \text{in regime 3,} \quad (18)$$

see equations (A.10, A.11, A.16, A.17, A.21, A.22) in Appendix A. The boundaries between the regimes are also defined in Appendix A (see also Fig. 6). Note that all three regimes of 'thin' fibrils correspond to low enough effective inter-ribbon attraction energies: $\tilde{\sigma} < \tilde{\sigma}_c$, where the upper boundary $\tilde{\sigma}_c$ (coming from the combined conditions (A.14, A.18, A.23)) depends on $\tilde{k}$ and is of the order unity.

In both *regimes 1 and 2* the equilibrium fibril twist strength is very close to the primary single-ribbon twist, $\gamma \simeq \gamma_0$. In *regime 1* it is the bending energy which stabilizes the growth of the fibril width, whereas in *regime 2* it is the twisting energy that determines the fibril diameter (see the corresponding terms in Eq. (7); both contributions increase with the number p of ribbons per fibril and compete with the attraction energy gain per ribbon $\mathcal{E}_{\rm attr}/p$, thus determining the optimal p). Hence, the fibril width p does not depend on $k_{\rm twist}$ in the asymptotic regime 1 (Eqs. (16)), and $k_{\rm bend}$ does not enter at all the results for the asymptotic regime 2, equations (17).

In contrast, in *regime 3* the equilibrium fibrils are considerably untwisted compared to the primary ribbons: $\gamma \ll \gamma_0$. The fibrils are composed of many ribbons ($p \gg 1$, see Eq. (A.25)), but the fibril width is still small if compared with the helix step: $\beta \ll 1$. This situation realizes only when the bending modulus exceeds the twisting one ($\tilde{k} \gtrsim 1$, see Fig. 6). The typical bending energy increment ($\partial\mathcal{E}_{\rm bend}/\partial\gamma \sim k_{\rm bend}\gamma^3(ap)^2$) and the increment of the twisting energy ($\partial\mathcal{E}_{\rm twist}/\partial\gamma \sim k_{\rm twist}\gamma_0$) for the ribbons in the equilibrium fibril are now of the same order (see Eqs. (7, A.21, A.22)), and the total elastic energy gain $\mathcal{E}_{\rm elast} \sim k_{\rm bend}\gamma^4(ap)^2$ (Eq. (7)) is now competing with (and equals to) the effective 'surface tension' term $\mathcal{E}_{\rm attr} \sim \sigma b/p$ (Eq. (9)), see equations (A.21, A.22).

For the case of *wide sheet-like fibrils* ($\beta \gg 1$) the asymptotic formulae (B.2) can be used and the consideration of Appendix B is appropriate. We distinguished between the case of wide but still finite and twisted sheet-like fibrils *(regime 4)* and the case of infinite, completely untwisted sheets *(regime 5)*. The case of 'thick fibrils' or 'wide stacks' is characterized by the following asymptotes (Eqs. (B.4)):

$$ap\gamma_0 \simeq \frac{2\pi\left(1+\tilde{k}\right)}{\left(\pi-\tilde{\sigma}\right)^2}; \quad \gamma \simeq \gamma_0 \frac{2\left(\pi-\tilde{\sigma}\right)}{\pi\left(1+\tilde{k}\right)} \quad \text{in regime 4.} \quad (19)$$

The above equations are valid if $0 < \pi - \tilde{\sigma} \ll 1$, see Figure 6. In this case the 'stack' is strongly untwisted compared to the primary ribbons, $\gamma \ll \gamma_0$.

For even higher effective attraction energy, $\tilde{\sigma} \geq \pi$, the ribbons tend to form infinite sheets (with null twist), *i.e.*

$$p \to \infty; \quad \gamma \to 0; \quad ap\gamma \to \infty \qquad \text{in regime 5} \quad (20)$$

(see Appendix B, Eqs. (B.7)).

The aggregates (fibrils) are stable if the net energy gain (when the ribbon enters a fibril) is negative, *i.e.* if $\mathcal{E} < 0$, *and* if $p \geq 2$. These two conditions are satisfied for

$$\tilde{\sigma} > \tilde{\sigma}_*, \quad (21)$$

where

$$\tilde{\sigma}_* \simeq \frac{2}{3}\tilde{k}\left(\gamma_0 a\right)^3 \quad \text{in regime 1} \quad (22)$$

$$\tilde{\sigma}_* \simeq \frac{16}{45}\left(\gamma_0 a\right)^5 \quad \text{in regime 2} \quad (23)$$

$$\tilde{\sigma}_* \simeq \frac{1}{2}\gamma_0 a \quad \text{in regime 3} \quad (24)$$

$$\tilde{\sigma}_* \simeq \frac{1}{2}\gamma_0 a - \frac{(\pi-\tilde{\sigma})}{2p} \quad \text{in regime 4} \quad (25)$$

$$\tilde{\sigma}_* = \frac{1}{2}\gamma_0 a \quad \text{in regime 5} \quad (26)$$

see equations (A.15, A.20, A.25, B.6, B.9). That means that the fibrils are stable only in a part of the diagram in Figure 6, namely above some boundary $\tilde{\sigma} > \tilde{\sigma}_*$ where $\tilde{\sigma}_*$ depends on $\tilde{k}$ and $(\gamma_0 a)$. The threshold $\tilde{\sigma}_*$ is not shown in Figure 6 due to the extra argument $(\gamma_0 a)$ involved, which cannot be reduced to just $\tilde{k}$ and $\tilde{\sigma}$.

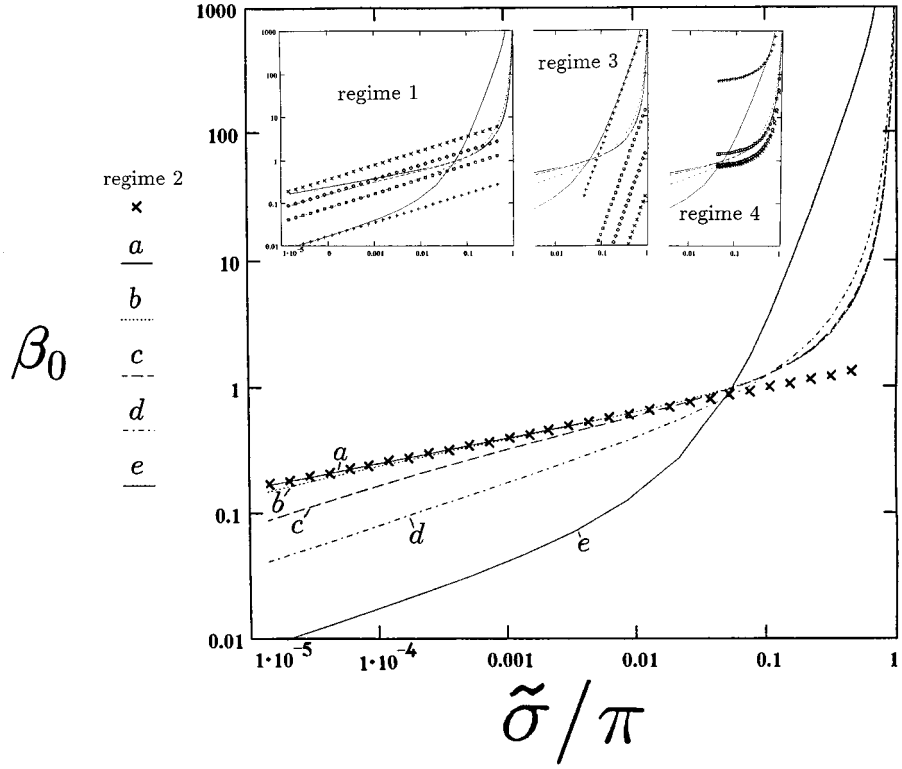

Fig. 7. The results of the numerical analysis of equations (13, 14) defining the equilibrium fibril structure. The plot shows the dependence of the normalized width of the fibrils, $\beta_0 \equiv pa\gamma_0/2$, on the normalized attraction energy $\tilde{\sigma}/\pi$. The ratio $\tilde{k} \equiv k_{\rm bend}/k_{\rm twist}$ is fixed along each line, the ratio $\tilde{\sigma} = \sigma ab/(\gamma_0 k_{\rm twist})$ varies from 0 to π (*i.e.* to the threshold of the regime 5 (infinite stacks)); $\tilde{k} = 0.001$ (a), 0.01 (b), 0.1 (c), 1 (d) and 100 (e). The line marked by crosses is plotted in accordance with equation (A.16), the asymptotic result in regime 2 ($\tilde{k} \ll 1$). The asymptotic results in the regimes 1 (the left inset, Eq. (A.10)), 3 (the middle inset, Eq. (A.22)) and 4 (the right inset, Eq. (B.3)) are also shown for $\tilde{k} = 0.01$ (crosses), 0.1 (diamonds), 1 (boxes) and 100 (pluses).

2.4 The general case

The system of equations (13, 14) was solved numerically in the cross-over regions separating the regimes considered in Section 2.3 above, and in particular for $\tilde{\sigma} \simeq 1$ (cross-over between the regimes 2, 3 and 4). Let us consider the effect of the attraction energy σ on the fibril formation ($\tilde{k} = $ const. and $\tilde{\sigma}$ is changing, see Eq. (11)). The results of the corresponding calculation are shown in Figures 7, 8 (it is still assumed that $p \gg 1$).

Figure 7 illustrates the reduced width of the fibrils, $\beta_0 \equiv pa\gamma_0/2$, as a function of the reduced attraction energy $\tilde{\sigma} \equiv \sigma ab/(\gamma_0 k_{\rm twist})$, and Figure 8 shows how the normalized equilibrium twist $\gamma/\gamma_0 \equiv \beta/\beta_0$ changes with $\tilde{\sigma}$. It is clear that the reduced width, β_0, is monotonously increasing with $\tilde{\sigma}$ for any $\tilde{k}$ (cp. Eqs. (16–19)). One can easily see that the fibril width tends to infinity as $\tilde{\sigma} \to \pi - 0$, and simultaneously the twist tends to zero (this is true for any $\tilde{k}$). For $\tilde{\sigma} \geq \pi$ the minimization of the free energy results in $p = \infty$, $\gamma \equiv 0$. For small enough $\tilde{\sigma}$ the fibril twist γ is very close to the initial twist γ_0 in an individual ribbon: $\gamma/\gamma_0 \simeq 1$. For small $\tilde{k}$ the twist γ first slightly increases and then decreases when $\tilde{\sigma}$ is increased (cp. Eqs. (16, 17)); γ always decreases with $\tilde{\sigma}$ for $\tilde{k} \gtrsim 1/2$.

Let us consider how the fibril structure depends on $k_{\rm bend}$ when all other parameters ($k_{\rm twist}$, σ, γ_0, a, b) are kept fixed, *i.e.* the dependence of the fibril structure on $\tilde{k}$ for fixed $\tilde{\sigma}$. The twist γ always decreases with increase of $\tilde{k}$ for any $\tilde{\sigma}$, see Figure 8. For small $\tilde{\sigma}$ (when thin enough fibrils are formed), an increase of $\tilde{k}$ (*i.e.* an increase of the bending modulus) at the beginning causes a decrease and then (for extremely high values of $\tilde{k} \gtrsim 1.5/\tilde{\sigma}^2$, Eq. (A.24)) an increase of the fibril width, see Figure 7. However, for larger $\tilde{\sigma}$ (namely, when $\tilde{\sigma}$ is close to the threshold π) an increase in $k_{\rm bend}$ always cause an increase of the width of fibrils and a decrease of twist (cp. Eqs. (19) for regime 4). In fact, a high bending modulus $k_{\rm bend}$ suppresses bend deformations, hence the ribbons have to untwist considerably in order to form a fibril.

One can easily check that numerical solutions of equations (13, 14) are in agreement with the asymptotic results discussed in Section 2.3. Indeed, in the limit of small $\tilde{\sigma}$ the asymptotes of the regime 1 are always approached, see the left inset in Figure 7 and the line $\gamma/\gamma_0 = 1$ (crosses) in Figure 8. For small $\tilde{k}$ and intermediate values of $\tilde{\sigma}$ it is equations (17) (regime 2) that are appropriate (see lines of crosses in Figs. 7, 8). For large enough $\tilde{k}$ and intermediate values of $\tilde{\sigma}$ the asymptotes of regime 3 are realized

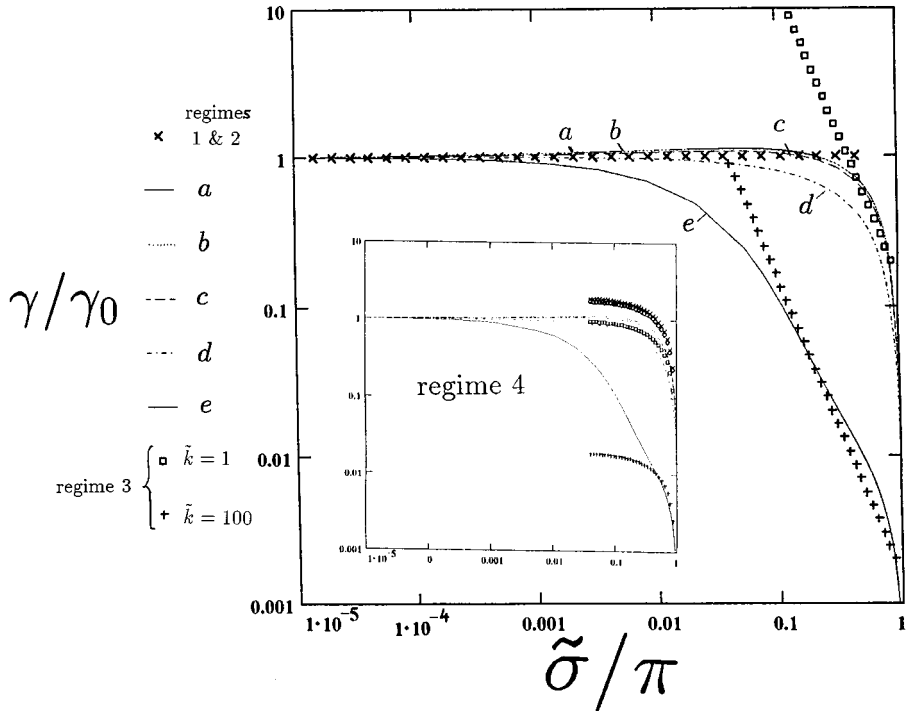

Fig. 8. The results of the numerical analysis of equations (13, 14) for the equilibrium fibril structure. The plot shows the dependence of the relative twist in equilibrium fibrils $\gamma/\gamma_0 \equiv \beta/\beta_0$ as a function of $\tilde{\sigma}/\pi$. The line marked by crosses corresponds to $\gamma/\gamma_0 = 1$ (the asymptotic result in regimes 1 and 2, Eqs. (A.11, A.17)), other lines show the asymptotic dependencies in regime 3, equation (A.21), for $\tilde{k} = 1$ (boxes) and 100 (pluses). The inset lines correspond to the asymptotic results in regime 4, equations (B.4). Other notations as in Figure 7.

(cp. the numerical results for $\tilde{k} = 100$ and the line of pluses in the middle inset of Fig. 7 and in the main part of Fig. 8). Finally, for $\tilde{\sigma}$ close to the threshold value π, the asymptotes of regime 4 are appropriate (the right inset of Fig. 7 and the inset of Fig. 8).

The question of fibril stability deserves an extra analysis. As was already mentioned above, the fibril is stable if the net fibril energy $\mathcal{E}$ (per ribbon) is negative. Using equation (10) this condition can be rewritten as

$$H > H_1 \equiv \frac{\beta}{4\tilde{\sigma}\beta_0^2}\left[\tilde{k}\left(C(\beta) - D(\beta)\right) + \left(C(\beta) + D(\beta)\right)\right] - \frac{C(\beta)}{\tilde{\sigma}\beta_0} + \frac{1}{2\beta_0} + \frac{1}{2\tilde{\sigma}} \tag{27}$$

where the left hand side represents the reduced twist step of the primary ribbon:

$$H \equiv \frac{1}{a\gamma_0} \equiv \frac{h_0}{2\pi a}\,. \tag{28}$$

The values β and β_0 are defined in equations (13, 14). The right hand side of condition 27, H_1, depends on the reduced molecular parameters $\tilde{k}$ and $\tilde{\sigma}$. Note that the larger is the primary twist step h_0, the weaker is the condition 27.

It is also important to check that $p \geq 2$, as the fibril must consist of at least two ribbons (a stronger condition, $p \gg 1$, was assumed above). Hence $p/2 \equiv \beta_0/(a\gamma_0) \geq 1$, *i.e.*

$$H \geq H_2 \equiv \frac{1}{\beta_0} \tag{29}$$

where β_0 is determined by equations (13, 14) (*i.e.* H_2 is a function of parameters $\tilde{k}$ and $\tilde{\sigma}$, like H_1). The right hand side of condition (29) is always a decreasing function of $\tilde{\sigma}$, see Figure 7.

The fibril is stable if $H > \max(H_1, H_2)$, or if the free energy of the minimal fibril is negative, $\mathcal{E}(p = 2) < 0$. The latter energy can be estimated using equation (10):

$$\frac{\mathcal{E}(p=2)}{\gamma_0^2 k_{\text{twist}}} = \min_{x \equiv a\gamma}\left\{\frac{x}{4\left(\gamma_0 a\right)^2}\left[\tilde{k}\left(C(x) - D(x)\right) + \left(C(x) + D(x)\right)\right] - \frac{C(x)}{\gamma_0 a} - \frac{\tilde{\sigma}}{2\gamma_0 a} + \frac{1}{2}\right\}. \tag{30}$$

The condition $\mathcal{E}(p = 2) < 0$ can be rewritten as $H > H_3$, where H_3 depends on $\tilde{\sigma}$, $\tilde{k}$.

Thus we arrive at the following general condition of fibril stability: $H > H_*$, where

$$H_* = \min\left(\max\left(H_1, H_2\right), H_3\right). \tag{31}$$

The effect of molecular parameters $\tilde{k}$ and $\tilde{\sigma}$ on the threshold H_* is illustrated in Figure 9.

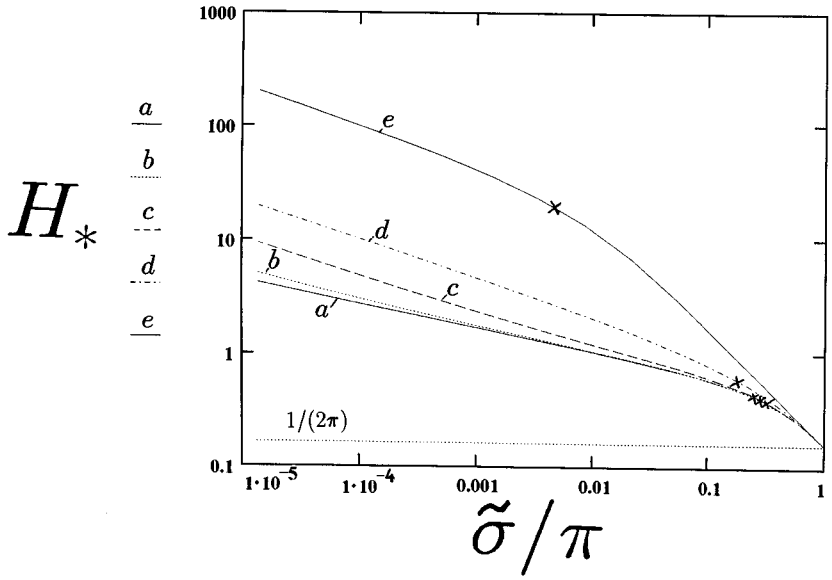

Fig. 9. The fibrils' stability threshold H_* (see Eq. (31)) as a function of the molecular parameter $\tilde{\sigma}/\pi$ for different values of $\tilde{k}$ as in Figures 7, 8: $\tilde{k} = 0.001$ (a), 0.01 (b), 0.1 (c), 1 (d) and 100 (e). The fibrils are stable if the reduced twist step of primary ribbons, H, is larger than H_*. The left parts of the curves are determined by the condition $H > H_3$, and the right parts – by the condition $H > H_1$ (the points where these conditions are equivalent are marked by crosses on each curve). It turns out that H_2 is always either lower than H_1, or it is higher than H_3, hence H_* is never determined by H_2. For $\tilde{\sigma} \geq \pi$ all curves merge to $H_* = 1/(2\tilde{\sigma})$ (see condition (B.9)).

One can easily see that H_* is a decreasing function of $\tilde{\sigma}$ for any $\tilde{k}$. Hence the fibrils are stable if $\tilde{\sigma} > \tilde{\sigma}_*(\tilde{k}, H)$, where the critical value $\tilde{\sigma}_*$ is implicitly defined in equation (31).

For $h_0 > a$ the fibrils are unstable if $\tilde{\sigma} < \tilde{\sigma}_*(\tilde{k}, H)$ (see Fig. 9). In the range $\tilde{\sigma}_*(\tilde{k}, H) < \tilde{\sigma} < \pi$ the equilibrium fibrils are finite: $2 \leq p < \infty$. Infinite sheets are formed instead of finite fibrils if $\tilde{\sigma} > \pi$.

On the other hand, finite fibrils are never stable if the primary twist strength is extremely (unrealistically) high: $h_0 < a$ (*i.e.* $1/H > 2\pi$); in this case single ribbons are stable if $\tilde{\sigma} < 0.5/H$, and infinite 'stacks' (sheets) are formed for higher inter-ribbon sticking energies, $\tilde{\sigma} > 0.5/H$.

One can clearly see that the smaller is the bending modulus (the smaller is $\tilde{k}$) and/or the weaker is the primary ribbon twist (the larger is h_0), the wider is the region of stability of the finite fibrils, see Figure 9.

3 Experimental

Standard automated solid phase method was employed for the synthesis of the 11-residue *de novo* DN1 peptide. The peptide was purified by reverse phase HPLC in water-acetonitrile gradient in the presence of 0.1% TFA (trifluoroacetic acid). Mass spectrometry confirmed the purity of the final product: the molecular mass is as expected $\mu = 1593$ [3]. The solutions under consideration are the DN1 peptide solution in a double distilled water.

The primary structure of DN1 peptide is: CH_3CO-Gln-Gln-Arg-Phe-Gln-Trp-Gln-Phe-Glu-Gln-Gln-NH_2. It was rationally designed to self-assemble into polymeric hydrogen-bonded β-sheet tapes in water. The $(\text{-}CH_2)_2$ moieties of the six glutamine residues are expected to provide attractive intermolecular hydrophobic interactions between side-chains. The residues Phe4, Trp6 and Phe8, which are also hydrophobic, are expected to provide additional intermolecular recognition due to $\pi-\pi$ interactions. Arg3 and Glu9 provide an additional degree of recognition *via* their strong Coulombic attraction (Arg being positive and Glu being negative for $4.1 < \text{pH} < 12.5$), and favour an antiparallel alignment of the strands. Chemically blocked peptide termini as well as doubled Gln's are used at the beginning and at the end of the peptide chain to reduce edge-to-edge Coulombic attraction between the tapes. Gln, Arg and Glu side-chains make one surface of the β-sheet tape more hydrophilic than the other; the latter is consisting of the side-chains Gln, Phe and Trp and is quite hydrophobic. Hence single β-sheet tapes combine into pairs (double tapes, *i.e.* ribbons). As a result, the DN1 peptide in water indeed forms double β-sheet tape-like structures (what is called *primary ribbons* or simply *ribbons* in other parts of this paper), see Figures 2a, 5a.

At higher concentrations the DN1 double tapes (ribbons) combine into *stacks* (*fibrils*) due to chemical affinity and geometric complementarity, Figures 2b, 5b. Indeed, the $-CONH_2$ moieties, in particular these at the end of the Glu side chains on the polar side of the single β-sheet which pave the outer sides of the double tapes, can establish an extensive hydrogen bond network between sides of the double tapes.

These fibrils then show a tendency to wind around each other to form rope-like fibres, Figure 2d. However, even the solutions which are half a year old, are apparently

not aged enough: formation of the rope-like fibres has not been accomplished for all fibrils. We believe that the driving force towards these rope-like structures is the attraction between the edges of the β-sheets forming the two opposite sides of the surface of the fibril as shown in Figure 5c.

Molecular modeling of the DN1 peptides inside the β-sheet structure yields the length of the peptide rod $b \simeq 37$ Å, its width along the β-sheet $c \simeq 4.7$ Å, and its width across the β-sheet $a_1 \simeq 10 \div 12.5$ Å (hence the width of the double tape is $a = 2a_1 \simeq 20 \div 25$ Å). That means that the concentration 1 mM $\simeq 1.6$ mg/ml corresponds to the volume fraction of about $0.12 \pm 0.01\%$ v/v (peptide density about 1.3 g/cm^3).

We possess an extensive experimental evidence showing that the self-assembling aggregates formed by the DN1 peptide in water are arranged locally similar to how it is cartooned in Figure 5. The basic structure formed by DN1 in water is an intermolecular β-sheet tape with antiparallel alignment of straight β-strands (without hairpins), Figure 1c. It is formed at high enough concentrations ($c > 75$ μM), and this β-sheet structure is an element of all higher order aggregates (double tapes, fibrils/fibres). This fact is proved by the analysis of infra-red and far-UV circular dichroism spectra as explained in references [3,4]. X-ray diffraction data reveal 4.7 Å periodicity in all structures and are consistent with the expected inter-strand distance in a β-sheet. The X-ray data are also consistent with the peptide β-strands being approximately perpendicular to the axis of fibrils [3].

The presence of two morphologically different kinds of self-assembling structures (ribbons and fibrils) is apparent from the transmission electron microscopy (TEM) images, Figures 2a, b, c (similar images were received from scanning electron microscopy and atomic force microscopy), it is also revealed in far- and near-UV CD spectroscopy. Indeed, the far-UV CD spectrum of the peptide tapes has a positive band at *ca.* 195 nm and a negative band at *ca.* 214 nm, features typical of β-sheet conformation. In contrast, the CD spectrum of fibrils has a shifted negative band, centered at 224 nm rather than at 214 nm. This shift is likely to arise from the superposition of a strong aromatic CD band on the classical CD spectrum which is associated with a change of stacking (to a more dense pattern) of the aromatic side-chains of the peptide molecules when they enter the fibrils, cp. references [9–11].

For TEMs Figure 2 the DN1 peptide solutions were incubated at a desired concentration for a long time to allow them to achieve equilibrium self-assembling structures. In all of the cases the starting peptide solutions were diluted to concentrations below 40 μM before imaging in order to prevent complete coverage of the grids by the peptide. The peptide solutions were immediately applied on freshly glow discharged, carbon-coated copper grids. The polymers were allowed to adsorb for 1 minute, followed by rinsing of the grids with distilled water, and air drying. The platinum rotary shadowing was carried out in a Balzer's apparatus, and the grids were examined using a Phillips CM100 electron microscope. Similar procedures were used for the preparation of the uranyl negative stained samples.

At very low concentrations DN1 peptide forms flexible chains (ribbons) less than 5 nm wide, with apparent length of the order of a micrometer, Figure 2a. The ribbons are observed when the starting solution for TEM was incubated at $c = 80 \div 600$ μM of DN1. Atomic force microscopy supports our model of two stacked β-sheet tapes as the structure of the ribbons (Fig. 5a): the apparent cross-section width of the ribbons is measured to variate between 20 and 40 Å (data not shown).

At higher concentrations ($c > 600$ μM) DN1 forms fibrils and fibres. The fibrils look like rigid rod-like polymers, *ca.* 8–10 nm wide, with apparent persistence length of the order of several dozens of micrometers, see Figure 2b. Their apparent contour length is of the order of micrometers, however we believe that this is the result of fibrils being broken down during preparation for TEM imaging, so that their actual length in solution may be significantly longer. If the diluted to $c \simeq 200$ μM solution of peptide fibrils is left at room temperature, over a course of several weeks, the fibrils are seen to unwind into several ribbons (double tapes). The width of the fibrils and the mass per unit length measurements support that the fibrils are made typically of stacks of approximately eight tapes (data not shown, in collaboration with Dr D. Holmes, Univ. Manchester).

It should be stressed that fibril/fibre dispersions of DN1 peptide are stable. Apart from sedimentation due to the density difference, no tendency to segregation from water was observed. Even having been aged for some two years, the DN1 solutions can restore their water-like homogeneity after a mild shaking with a hand.

4 Estimation of the molecular parameters for water solutions of DN1 peptide ribbons

In this section we estimate a number of molecular parameters of the DN1 ribbons and the fibrils formed by the ribbons using the theory presented in Section 2. We assume that the primary ribbons (structural units of the fibrils) are the *double* tapes for the DN1 in water: as explained in Section 3, one side of a single DN1 tape is strongly hydrophobic, hence favouring a formation of paired (doubled) tapes; single tape fragments must be unfavourable. This assumption is supported by the UV CD spectra analysis and the TEM photographs, as explained in references [5,6].

Molecular dimensions of one peptide molecule in a rod-like (extended β-strand) conformation (inside β-sheet) are (see Sect. 3):

$$a_1 \simeq 11.5 \text{ Å}; \quad b \simeq 37 \text{ Å}; \quad c \simeq 4.7 \text{ Å}, \tag{32}$$

hence the double tape (the ribbon) has a cross-section $a \times b$ with $a \simeq 2a_1 \simeq 23$ Å. c is the distance between the peptide molecules ('rods') in a tape along its main axis, see Figures 1d, 4, 5a.

Let us consider the bend and twist energies starting with single β-sheet tapes. Neighbouring peptide molecules in each DN1 β-sheet are connected into tape by 11 hydrogen bonds and other attractions as explained in Section 3. We characterize these bonds/attractions with effective springs between the neighbouring rods assuming that the effective bonds are homogeneously distributed along the rods. A tape deformation causes additional separation δR between the monomers connected by the bonds, so the energy of all bonds between a pair of rods neighbouring in the tape is

$$\delta E = \frac{\varkappa}{2} \int (\delta R(x,y))^2 \, \mathrm{d}x\mathrm{d}y \tag{33}$$

where $\varkappa$ is the elastic constant, x is the coordinate of a relevant chemical unit along the rod axis, $-b/2 < x < b/2$, y is the coordinate across the tape ($-a_1/2 < y < a_1/2$) and $\delta R(x,y)$ is the variation of the radius-vector connecting units involved in the chemical bond at the point (x,y)[7]. If a single β-sheet is twisted with a twisting strength γ (this corresponds to a twisting angle $\theta = \gamma c$ per rod, cp. Eqs (5, 6), and $\delta R(x,y) \simeq \theta x$) the energy per rod is $\delta E = \varkappa(\gamma c)^2 b^3 a_1/24$. If a single β-sheet is bent with curvature ν (the bending angle is hence $\tilde{\theta} = c\nu$ per each rod step, see Eq. (2)), the separation is $\delta R = \tilde{\theta} y$. Hence the energy per rod is $\delta E = \varkappa(\nu c)^2 a_1^3 b/24$.

Two tapes are stuck into a ribbon (double tape) by hydrophobic attraction between the side groups of peptides (lining one of the sides of each single tape). We first assume that this attraction is homogeneous and is not related to the positions of particular rods inside the tapes, *i.e.* that single tapes freely slide along each other to adjust their length when the double tape is bent[8]. Hence the energy increment for a double tape $\delta E_\mathrm{d} = 2\ \delta E$. Comparing the energy increments, δE_d, for twisted and bent tapes (see above) with the definitions given in equation (4) we get the following equations for bending and twisting constants of double tapes:

$$k_\mathrm{bend} = \varkappa a_1^3 bc/6 \tag{34}$$

$$k_\mathrm{twist} = \varkappa a_1 b^3 c/6. \tag{35}$$

The ratio of the moduli is

$$\tilde{k} \equiv \frac{k_\mathrm{bend}}{k_\mathrm{twist}} = \left(\frac{a_1}{b}\right)^2 \simeq 0.1. \tag{36}$$

From the electron micrographs of fibrils we see that $h \simeq 1600 \pm 400$ Å, see Figures 2c, d, *i.e.* $\gamma = 2\pi/h \simeq (4 \pm 1) \times 10^{-3}$ Å^{-1}. The fibril diameter (ap) is approximately 90 ± 10 Å corresponding to $p \sim 4$ of double tapes in a fibril (see Eq. (32)), and the twist parameter $\beta \equiv \gamma ap/2 \simeq 0.18 \pm 0.05$ (see Eq. (11)) is rather small, so the equations for regimes 1 or 2 are applicable in the first approximation (see Sect. 2.3). Regime 3 is excluded since $\tilde{k} < 1$ (see Eq. (36) and Fig. 6). Hence $\gamma \simeq \gamma_0$ (see Eqs. (16, 17)), *i.e.*

$$\gamma_0 \simeq (4 \pm 1) \times 10^{-3} \text{ Å}^{-1}. \tag{37}$$

Note that the typical twisting angle per rod in DN1 primary double tape, $\theta \simeq c\gamma_0 \simeq 0.02 \sim 1°$, is small if compared with the typical twist angles in most native primary β-sheets (about $10 \div 30°$, Refs. [1,2]). The fact that this twist is so weak promotes the effective fibrillization of the DN1 ribbons (see Fig. 9 and the discussion at the end of Sect. 2.4).

Using the obtained values $\beta_0 \equiv \gamma_0 ap/2 \simeq \beta \simeq 0.18$ and $\tilde{k} \simeq 0.1$, we can verify that the system falls into the first regime: solving the first equation (16) for $\tilde{\sigma}$ we get the reduced sticking energy

$$\tilde{\sigma} \equiv \frac{\sigma ab}{\gamma_0 k_\mathrm{twist}} \simeq 4 \times 10^{-4} \tag{38}$$

which is consistent with the condition (A.14) specifying regime 1.

The persistence length $\tilde{l}^{(2d)}$ of DN1 ribbons (double tapes) in two dimensions (on the surface) can be estimated using the electron micrographs (Fig. 2a) obtained at very low concentrations where the fibrils are split into separate double tapes: $\tilde{l}^{(2\mathrm{d})} \simeq (0.8 \div 3.5) \times 10^4$ Å $\sim 2 \times 10^4$ Å. On the other hand, the apparent persistence length of a twisted tape confined to a surface can be related to its elastic moduli; assuming that $k_\mathrm{splay} \gg k_\mathrm{bend}$ we get

$$\tilde{l}^{(2\mathrm{d})} = \frac{4k_\mathrm{bend}}{k_\mathrm{B}T} \tag{39}$$

(it is twice its persistence length in three dimensions $\tilde{l}^{(3\mathrm{d})} = 2k_\mathrm{bend}/k_\mathrm{B}T$, and the latter one is again twice the persistence length l_pers of an ordinary semiflexible polymer with $k_\mathrm{bend} \simeq k_\mathrm{splay} = k$ in 3d-space: $l_\mathrm{pers} = k/k_\mathrm{B}T$ [12]). Hence we obtain the following estimate for the bending modulus

$$\frac{k_\mathrm{bend}}{k_\mathrm{B}T} \sim 0.5\ \mu\mathrm{m}. \tag{40}$$

Using equation (36) we also get the twisting modulus:

$$\frac{k_\mathrm{twist}}{k_\mathrm{B}T} \sim 5\ \mu\mathrm{m}, \tag{41}$$

and, finally, the energy of the inter-ribbon attraction (see Eqs. (32, 37, 38)):

$$\frac{\sigma}{k_\mathrm{B}T} \sim 10^{-4}\ \text{Å}^{-2} \tag{42}$$

i.e. the sticking energy per rod is $\sigma bc \sim 0.015\ k_\mathrm{B}T$ and the sticking energy per persistence length $\tilde{l}^{(3\mathrm{d})}$ is high: $\sigma b \tilde{l}^{(3\mathrm{d})} \sim 30\, k_\mathrm{B}T$.

[7] Isotropic model is assumed here for simplicity: the elastic energy increment is assumed to be independent of the direction of $\delta\mathbf{R}$ vector.

[8] The opposite assumption is that the two tapes are structurally linked by the side-chains into the ribbon, the difference is explained in the end of this section, see equations (43, 45).

Above we have adopted an extreme assumption of homogeneous attraction between the tapes in the ribbon (hence, $\delta E_{\rm d} = 2\,\delta E$). The opposite extreme assumption is that the two tapes are structurally linked by the side-chains into a crystal-like ribbon. In this latter case, we can apply the same model of homogeneously distributed isotropic bonds (between consequent c-segments) to the ribbon as a whole, as used above for single tapes. Hence,

$$k_{\rm bend} = \varkappa a^3 bc/12, \qquad k_{\rm twist} = \varkappa a b^3 c/12, \tag{43}$$

i.e. $k_{\rm bend}$ is now four times higher than it was before, and hence now $\tilde{k} = (a/b)^2 \simeq 0.4$ (cp. Eqs. (34, 35, 36)). Note that as before: $\tilde{k} < 1$, hence equation (37) for γ_0 still holds. Equation (40) for the value of the bending modulus $k_{\rm bend}$ holds as well, being directly related to the experimental value of persistent length of the ribbons $\tilde{l}^{(2{\rm d})}$. Therefore, the new values for $k_{\rm twist}$ and $\tilde{\sigma}$ (cp. Eqs. (38, 41)) are:

$$\frac{k_{\rm twist}}{k_{\rm B}T} \simeq 1.25\ \mu{\rm m}, \quad \tilde{\sigma} \simeq 1.6 \times 10^{-3} \tag{44}$$

(see Eqs. (11, 16, A.14), in particular condition (A.14) verifies that the system still falls well into the first regime). Finally, applying equations (32, 37, 45) we get the same equation (42) for the sticking inter-ribbon energy σ.

Combining the results for both extreme assumptions considered above, we thus conclude that the DN1 peptide ribbons are characterized by the following parameters:

$$\gamma_0 \equiv \frac{2\pi}{h_0} \simeq 4 \times 10^{-3}\ {\rm \AA}^{-1}; \qquad \sigma bc \simeq 0.015 k_{\rm B}T;$$
$$\frac{k_{\rm bend}}{k_{\rm B}T} \simeq 0.5\ \mu{\rm m}; \qquad \frac{k_{\rm twist}}{k_{\rm B}T} \simeq 1.25 \div 5\ \mu{\rm m}. \tag{45}$$

5 Discussion and conclusions

A theory for equilibrium fibrils being formed in solutions of self-assembling peptides is proposed. The primary self-assembling structure in these solutions is a β-sheet tape which is twisted due to L-chirality of the peptides forming the β-sheet (Figs. 1c, d, 4a). These primary tapes (ribbons) combine into fibrils, the latter being stacks of tapes stuck together due to face-to-face attraction between their longer sides, Figures 1f, 4b. For untwisted tapes (ribbons) infinitely wide stacks formation is anticipated, Figure 3a. However, for the twisted tapes the growth of fibril width is restricted by the penalty arising from elastic distortions of the tapes when they enter a fibril. The width of the fibrils is thus stabilized by their intrinsic twist.

Our theory allows to describe the fibril structure in terms of geometrical parameters of primary ribbons (their cross-section $a \times b$ and their intrinsic twist strength $\gamma_0 \equiv 2\pi/h_0$, where h_0 is the twist period), their elastic constants ($k_{\rm bend}$ and $k_{\rm twist}$), and the energy of inter-ribbon face-to-face attraction (σ), see equations (13, 14, 16–19).

Fibrils are formed if the attraction energy is higher than some threshold, $\tilde{\sigma} > \tilde{\sigma}_*$ (here $\tilde{\sigma} \equiv \sigma ab/\gamma_0 k_{\rm twist}$), which is vanishing in the limit of low twist: $\tilde{\sigma}_* \to 0$ as $h_0/a \equiv 2\pi H \to \infty$ (Fig. 9 and Eq. (31)). The region of stable fibrils is wide when the primary ribbons are not strongly twisted and the ratio $\tilde{k} \equiv k_{\rm bend}/k_{\rm twist}$ is small.

If the attraction energy is very high ($\tilde{\sigma} > \pi$), infinite sheets of stacked ribbons are formed instead of fibrils, as shown in Figure 3a. In this structure, the ribbons are completely untwisted, the bend energy of the ribbons is null, and the twist energy penalty is compensated by inter-ribbon face-to-face attraction.

The calculated dependencies of the fibril parameters on the molecular constants of primary ribbons are shown in Figures 7, 8, 9. The scaling diagram of possible fibril structures is shown in Figure 6.

For a particular case of DN1 synthetic peptide, the primary ribbon is a double β-sheet tape (see Fig. 5a and Sect. 3). Such double tapes dominate in DN1 water solution for intermediate concentration range (100 μM $< c <$ 600 μM), Figure 2a. For higher concentrations, fibrils (Fig. 5b) are formed, they are imaged in Figure 2b. Our theory allowed to estimate the molecular parameters of the primary (double β-sheet) DN1 ribbons from the observed geometrical characteristics of the ribbons and fibrils (see Sect. 4, Eqs. (45)).

In some cases a further self-organization takes place: the DN1 fibrils are seen to wrap around each other to form rope-like fibres, see Figure 5c and reference [5]. The driving force for rope formation is the edge-to-edge attraction between β-sheets forming the fibrils. Similarly to fibril stabilisation, the size of the rope (the number of the fibrils per rope) is restricted by the elastic penalty due to distortions of the fibrils upon coiling around each other.

The phenomenon of fibril/fibre formation provides a unique example of micellization which is controlled by twist instead of being controlled by amphiphilic nature of aggregating molecules. Like a micellization emerging at the critical micelle concentration, the fibril formation takes place at some particular concentration, where the primary ribbon population saturates. Fibril diameter is determined by a balance between ribbon attraction and elastic distortion penalty, thus it is nearly independent of peptide concentration.

The driving force for ribbon stacking into fibrils, which was considered so far, is a specific attraction between the wider sides of the primary ribbons (*e.g.* for the case of DN1 it was an extensive hydrogen bond network between the ends of the Glu side chains, see Sect. 3). For this attraction to be effective enough (to stabilize fibrils from splitting into separate ribbons), a direct contact between faces of the neighboring tapes is needed. This requirement ensures that tapes in the fibril are intertwisted, as shown in Figure 4b.

The fibrils are bulky stiff objects, Figure 2b. Yet, DN1 fibril dispersions proved to be stable (see Sect. 3). This may sound surprising in view of the fact that usually van der Waals interactions (and other, *e.g.* hydrophobic, hydrogen binding, etc. attractive interactions) result in precipitation of stiff rod-like objects (nematic mesogens, viruses, surfactant cylindrical micelles, etc.). There is, however, a crucial difference between a solution

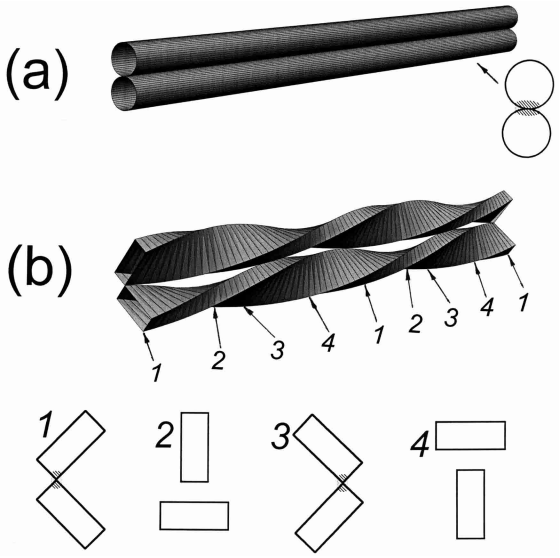

Fig. 10. Cylinders *vs.* screw-like fibrils: 3d views and some cross-sections. Parallel cylinders (a) can be put in contact along all of their length, whereas fibrils (b) always touch each other only occasionally (cross-sections *1* and *3*). The effective interaction areas (related to some short-range interactions, like *e.g.* van der Waals one, cp. Ref. [13]) are shadowed in the cross-sections. Geometrical parameters (in Å) of the bodies as illustrated in this picture: the fibrils (b) have cross-section $(D_1 = 40) \times (D_2 = 100)$ and twist period $h = 1600$ (similar to the DN1 fibrils), the cylinders (diameter $D_0 \simeq 71.4$) (a) have the same cross-section area ($\pi D_0^2/4 = D_1 D_2$). The inter-axis distances D_Δ are chosen to ensure the most close packing: $D_\Delta = D_0$ (a) and $D_\Delta = (D_1 + D_2)/\sqrt{2} \simeq 100$ (b); the upper fibril in (b) is shifted by $h/4$ along its axis with respect to the lower one to ensure minimal inter-axis distance.

of cylinders and a solutions of fibrils of similar width and rigidity. The difference comes from the local geometry of the fibrils when they approach each other. Indeed, the effective "interaction area" [13] between two cylinders is typically much larger than that for fibrils, as illustrated in Figure 10. This results in a *much weaker attraction between fibrils* compared to that for cylinders. This difference in attraction energies can be evaluated for *e.g.* a classical nonretarded van der Waals pair potential ($\propto r^{-6}$): the interaction energy for cylinders scales as $W_{\rm cyl}^{\rm attr} \sim AL\frac{D^{1/2}}{d^{3/2}}$ [13] (a) and $W_{\rm fib}^{\rm attr} \sim A\frac{L}{D}\ln\left(\frac{D_1}{d}\right)$ for fibrils[9] (b), where A is the so called Hamaker constant, d is the minimum gap between the bodies[10], D is the cylinder diameter or the typical width of the fibril, and L is the length of the parallel cylinders/fibrils (here we assume that the cylinders/fibrils are absolutely rigid); it is clear that for the same A:

$$W_{\rm fib}^{\rm attr}/W_{\rm cyl}^{\rm attr} \equiv \mathcal{R}_{\rm fib/cyl} \sim (d/D)^{3/2}\ln(D_1/d) \ll 1. \quad (46)$$

Hence, twisted fibrils can form stable dispersions, whereas similar rod-like molecules aggregate and precipitate from the solution, despite the entropic repulsion[11] and/or Coulombic repulsion.

We showed that under reasonable conditions the fibril state does correspond to the lowest free energy, so that fibril formation must be generally expected if the primary self-assembled ribbons are not very short, *i.e.* if the peptide concentration is not extremely low. The structure of the fibrils is determined by the properties of the primary ribbons only and hence is not concentration dependent. The fibril structure in turn is a source of information on the primary β-sheet parameters (as demonstrated in Sect. 4). However, the fibril formation from the primary β-sheet ribbons is likely to be kinetically hindered. Hence a (temporary) significant increase of peptide concentration or seeding by already formed fibril fragments might

[9] To estimate the van der Waals attraction energy $W_{\rm fib}^{\rm attr}$ between two absolutely rigid parallel fibrils, we assume that $h \gg D_2 \geq D_1$, introduce z axis along the fibril axes ($z = 0$ for the cross-section *'1'* and $z = h/8$ for *'2'* in Fig. 10b) and note that for $|z| \ll h$ the rectangular cross-sections may be regarded as quarter-planes with a small gap $\Delta(z)$ between their corners: $\Delta(z) \sim d + \frac{2\pi}{h} D\,|z|$, where $D = (D_1 + D_2)/\sqrt{2}$. Hence, attraction energy per unit fibril length is approximately

$$\mathrm{d}W/\mathrm{d}z \sim A \int .. \int_0^{+\infty} \left(\Delta^2(z) + (x_1 + x_2)^2 + (y_1 + y_2)^2\right)^{-5/2} \mathrm{d}x_1 \mathrm{d}x_2 \mathrm{d}y_1 \mathrm{d}y_2 \sim A/\Delta(z)$$

and finally $W_{\rm fib}^{\rm attr} \sim (Ah/D)\ln(D_1/d)$ for fibril fragment of length $\delta z = h/4$. That gives the estimate $W_{\rm fib}^{\rm attr}/L \sim (A/D)\ln(D_1/d)$, as in text.

[10] The gap d equals to the lattice atomic size ($d \simeq 2$–4 Å) for unsolvated bodies or to the double width of the hydration shells for the case when the bodies are solvated.

[11] Real chains (cylinders or fibrils) are never absolutely rigid; hence, an entropy penalty due to their aggregation (in order to retain their contact along long distance), resulting in the *entropic repulsion*; corresponding free energy is of the order $W^{\rm rep} \sim L\, k_{\rm B}T \left(d^2\tilde{l}\right)^{-1/3}$, $\tilde{l}$ is persistence length of the chain, cp. reference [14]. Semi-rigid objects (cylinders or fibrils) do not precipitate, if $W^{\rm attr} < W^{\rm rep}$. The latter condition gives us an estimate for the precipitation threshold value of the Hamaker constant A^* (in the absence of other repulsions). The ratio of such threshold values for fibrils *vs* cylinders is: $A_{\rm fib}^*/A_{\rm cyl}^* \simeq \mathcal{R}_{\rm fib/cyl}^{-1} \gg 1$ (see Eq. (46)) for the chains with the same persistence lengths $\tilde{l}$ and the same d and D. In particular, for cylinders $A_{\rm cyl}^* \simeq$ const. $\times\, k_{\rm B}T(d^5 D^{-3}\tilde{l}^{-2})^{1/6}$ with const. $= 24\sqrt{2}$ (see Ref. [13] for exact numerical coefficient in $W_{\rm cyl}^{\rm attr}$), which results in $A_{\rm cyl}^* \simeq 5 \times 10^{-22}$ J for $\tilde{l} = 50$ μm, $d = 3$ Å, $D = 70$ Å ($T = 300$ K). For fibrils with $d = 3$ Å, $D_1 = 40$ Å, $D_2 = 100$ Å (cp. Fig. 10) and the same $\tilde{l} = 50$ μm (cp. DN1 fibrils in Fig. 2b): $A_{\rm fib}^* \simeq \mathcal{R}_{\rm fib/cyl}^{-1}\, A_{\rm cyl}^* \sim 3 \times 10^{-20}$ J. Note that the typical values of Hamaker constant for interactions of solid (liquid) bodies across another liquid are within the range of $10^{-21} - 10^{-20}$ J, *e.g.* $A \sim (3-9) \times 10^{-21}$ J for interactions of hydrocarbons across water [13]. That means that for a typical A: $A_{\rm cyl}^* < A < A_{\rm fib}^*$.

be necessary in order to start the fibrillization in a dilute solution. One reason for such kinetic hindering comes from the fact that the primary ribbons are twisted and thus cannot simply zip up into a fibril as the ribbons in a fibril are strongly entangled (winded around each other). A new ribbon should either 'screw' into the growing fibril, or it has to split into short fragments in order to overcome topological restrictions. Both ways imply high potential barriers. To further discuss this point we have to estimate the ribbon scission energy and other parameters relevant for the β-sheet and fibril formation processes. This will be the subject of a separate publication.

After we have observed fibril formation in our model DN1 peptide solutions and formulated the principle of twist stabilisation, we found a huge variety of systems where fibrils of a well-defined diameter are formed. Below we list some of them, for which the twist stabilisation may play a crucial role.

We begin with peptide β-sheet forming systems which are directly comparable to DN1. Fibril/fibre formation observed in DN1 peptides looks very similar to the fibrillization which is characteristic for a number of the so called amyloidosis diseases including many incurable disorders (Alzheimer's diseases, Parkinsonism, prions, arthritises, haemodialysis, etc.) [15]. In each case some peptides start forming β-sheet structures which later combine into fibrils/fibres, that inhibit the normal living functions of the surrounding cells. Native amyloid fibrils (protofibrils) are believed to consist of a few (2-4) stacked face-to-face, twisted β-sheet tapes, whereas amyloid fibres are bundles formed by fibrils that are intertwisted like in a rope [16] (cp. Figs. 5b, c). In all the cases, protofibrils and bundles have well-defined diameters, in agreement with the general consideration of Section 2. In particular, various specially selected fragments of amyloid peptides sometimes form 'ribbon-like' fibrils which have very high stacking numbers p ($p > 100$) [17], *i.e.* they comprise of hundreds of β-sheet layers stacked together; this structure resembles the one predicted in regime 4 of the diagram in Figure 6. Among other twisted aggregates with well-defined diameters formed from β-sheet peptides are: fibres made of twisted filaments formed by many specific silk proteins [18], β-1,3-glucan microfibrils that are capable of further self-assembling into thick fibrils found in regenerating cell walls of yeast [19], fibrous polymers formed by polyglutamine-containing peptide fragments associated with Huntington disease [20], insulin [21], glucagon [22] and many other amyloid-like fibrils including the aggregates produced with enzymes or enzyme inhibitors [23].

The *generic mechanism* of *fibril stabilization by twist* works in the following way: If the primary building blocks are chiral and are capable of aggregation into chain-like structures, these primary chains will be chiral (twisted) as well. If in turn, these chains aggregate laterally into stacks or bundles, so that the aggregation attraction energy comes into effect only when the primary chains touch each other with their complementary sides, then the chains will have to intertwist in order to gain the attraction energy, and hence elastic energy penalty has to be paid for the fibril formation. The thicker the fibril, the higher the elastic penalty. This serves to stabilize the fibril diameter growth.

This mechanism can be applied to cellulose microfibrils (crystallites), which appear to be the basic structural element of the native cellulose [24]. Rope-like fibrils ('corkscrew' columns, 'threads', 'M-ribbons') are found in solutions of so called chromonics (column-forming molecules, usually of flat disk-like aromatic structure, such as those used as dyes or for medication, or as cholesteric liquid crystals) in the presence of chiral additives (or if the molecules are chiral themselves) [25–28]. In sickle-cell hemoglobin (HbS) anemia disease, deoxyHbS molecules (each shaped as a droplet with specific complementary-interacting points) aggregate into helical double chains which in turn form fibrils consisting of seven such double chains [29]. Chiral lipid bilayers [30], and non-chiral bilayers in the presence of chiral counter-ions [31], or in the presence of the channel-forming α-helix peptides [32] do stack together and form twisted ribbon-like fibrils. Extended range of hierarchical fibrillar structures (protofibrils which form fibrils, these fibrils in turn stack together either into "fibril-ribbons" (transforming into tubes), or at other conditions into "cables") are found in solutions of calcitonin peptide hormone [23]. Complementary associating derivatives of tartaric acid [33], or of chiral 1,2 diaminocyclohexane with (S,S)1,2-cyclohexanol [34], substituted porphyrins and phthalocyanines [35], derivatives of carbohydrates [34] and cholesterol [35,36], lithium salts of D (or L)-12-hydroxystearic acid [35], N-n-octyl-D-gluconamide [34,37], copper β-diketonates [35], chiral cyclohexanediamides [38], all of them do form some helical polymeric aggregates. In all of these cases, perfect twisted fibrils of fixed width are found and the primary chains can be easily distinguished to be far too thin to expect any other mechanism of stabilisation (*e.g.* amphiphilic stabilisation) apart from the stabilisation by twist. The twist stabilisation mechanism is possibly also applicable (although kinetic reasons cannot be excluded) to helical polyacetylene fibrillar morphologies formed with a chiral nematic reaction field [39].

We thank T. McLeish for useful discussions on the topic of the paper. The work was supported by the UK Engineering and Physical Sciences Research Council (GR/L37694 and GR/L34983). One of us (AA) wishes to thank the Royal Society for the award of a Dorothy Hodgkin Fellowship.

Appendix A: The asymptotic limit of thin fibrils (small β)

For thin enough fibril,

$$\beta = \frac{ap\gamma}{2} \ll 1 \tag{A.1}$$

we can represent all functions in Section 2.2 as truncated series of β. It is more convenient to start with the free

energy in the form (10); the essential term in curly brackets can be approximated as (we use variables γ and p for convenience here)

$$\frac{\tilde{k}}{24}(ap)^2\frac{\gamma^4}{\gamma_0^2}\left(1-\frac{3}{10}(ap\gamma)^2\right)+\frac{1}{2}\left(\frac{\gamma}{\gamma_0}-1\right)^2 - \frac{1}{2}-\frac{1}{12}(ap)^2\frac{\gamma^3}{\gamma_0}\left(\frac{\gamma}{\gamma_0}-1\right) + \frac{(ap)^4}{160}\frac{\gamma^5}{\gamma_0}\left(3\frac{\gamma}{\gamma_0}-2\right)+\frac{\tilde{\sigma}}{ap\gamma_0}\cdot \quad (A.2)$$

The minimization of equation (A.2) over γ and p produces the following system of equations:

$$\frac{(ap\gamma)^2}{6}\left[\frac{\gamma}{\gamma_0}\left(\tilde{k}-2\right)+\frac{3}{2} -\frac{9}{20}(ap\gamma)^2\left(\frac{\gamma}{\gamma_0}\left(\tilde{k}-\frac{3}{2}\right)+\frac{5}{6}\right)\right]=\frac{\gamma_0-\gamma}{\gamma_0} \quad (A.3)$$

$$(pa\gamma_0)^3\left[\tilde{k}+2\left(\frac{\gamma_0}{\gamma}-1\right)+\frac{3}{5}(pa\gamma_0)^2\left(\frac{\gamma}{\gamma_0}\right)^2 \times\left(-\tilde{k}+\frac{3}{2}-\frac{\gamma}{\gamma_0}\right)\right]=12\tilde{\sigma}\left(\frac{\gamma_0}{\gamma}\right)^4\cdot \quad (A.4)$$

Let us analyse these equations (which should be solved for γ and p) in some asymptotic regimes.

A.1 Regime 1

The simplest situation is when the left hand side of equation (A.3) is small compared to unity (note that it contains a small factor $ap\gamma$, Eq. (A.1)), hence

$$\gamma\simeq\gamma_0 \quad (A.5)$$

and

$$\frac{\gamma_0-\gamma}{\gamma_0}\simeq\frac{(ap\gamma_0)^2}{6}\left[\tilde{k}-\frac{1}{2}-\frac{9}{20}(ap\gamma_0)^2\left(\tilde{k}-\frac{2}{3}\right)\right] \quad (A.6)$$

$$12\tilde{\sigma}\simeq(ap\gamma_0)^3\left[\tilde{k}+2\left(\frac{\gamma_0}{\gamma}-1\right)-\frac{3}{5}(ap\gamma_0)^2\left(\tilde{k}-\frac{1}{2}\right)\right]. \quad (A.7)$$

One can easily check that the solution to these equations does not show any singularity at $\tilde{k}\simeq 1/2$. Hence we can safely assume that

$$\left|\tilde{k}-1/2\right|\gtrsim(ap\gamma_0)^2 \quad (A.8)$$

(which is true in practice, see Eq. (36)). Assuming also that $\tilde{k}$ dominates over other terms in the square brackets in equation (A.7):

$$\tilde{k}\gtrsim\left|\frac{\gamma_0}{\gamma}-1\right|,\quad \tilde{k}\gtrsim(ap\gamma_0)^2\left|\tilde{k}-\frac{1}{2}\right|, \quad (A.9)$$

we get the following solution to equations (A.6, A.7):

$$pa\gamma_0\simeq\left(\frac{12\tilde{\sigma}}{\tilde{k}}\right)^{1/3} \quad (A.10)$$

$$\frac{\gamma_0-\gamma}{\gamma_0}\simeq\left(\frac{12\tilde{\sigma}}{\tilde{k}}\right)^{2/3}\frac{\tilde{k}-1/2}{6} \qquad \text{in regime 1} \quad (A.11)$$

(we used the condition (A.8) here)[12]. The results above are true as long as conditions (A.1, A.5, A.9) are satisfied, *i.e.*

$$\tilde{\sigma}\ll\frac{2}{3}\tilde{k} \quad (A.12)$$

$$\tilde{\sigma}\ll\left(\frac{3}{2\tilde{k}}\right)^{1/2} \quad (A.13)$$

$$\tilde{\sigma}\ll\begin{cases}\dfrac{5\sqrt{15}}{32}\tilde{k}, & \text{if } \tilde{k}\gtrsim\frac{1}{2};\\ \dfrac{5}{8}\left(\dfrac{15}{2}\tilde{k}^5\right)^{1/2}, & \text{if } \tilde{k}\lesssim\frac{1}{2}.\end{cases} \quad (A.14)$$

One can easily check that conditions (A.14) are stronger than condition (A.12). Thus the corresponding *regime* 1 (see Fig. 6) is defined by inequations (A.13, A.14).

The fibrils are stable if $\mathcal{E}<0$ and $p\geq 2$, *i.e.* if

$$\tilde{\sigma}\gtrsim\frac{2}{3}\tilde{k}(\gamma_0 a)^3 \qquad \text{in regime 1} \quad (A.15)$$

(see Eqs. (10, A.10)). Note that $a\gamma_0=2\pi a/h_0$ is usually small, hence a small enough $\tilde{\sigma}$ may be compatible with the condition (A.15).

A.2 Regime 2

Now we start again with equations (A.6, A.7). In accordance with equation (A.6) the second and the third terms in the square brackets of equation (A.7) are of the same order (note the condition (A.8)). Let us now assume that these two terms dominate over $\tilde{k}$ in equation (A.7) (note that this assumption implies that $\tilde{k}$ must be small). For this case the system of equations (A.6, A.7) has the following solution:

$$pa\gamma_0\simeq(90\tilde{\sigma})^{1/5} \quad (A.16)$$

[12] Note that for small $\tilde{k}<0.5$ the resulting fibril twist γ, equation (A.11), is *larger* than γ_0. However the outer ribbons in the fibril have effective twist $\gamma/(1+\gamma^2\rho_j^2)$ which is still smaller than γ_0 (see Eq. (7)): for $\tilde{k}\ll 1$ and $\rho_{\max}\simeq ap/2$ the effective twist is $\gamma/(1+\gamma^2a^2p^2/4)\simeq\gamma_0\left(1-(1/6)(12\tilde{\sigma}/\tilde{k})^{2/3}\right)<\gamma_0$, see equations (A.10, A.11). One can easily check using equations (5, 7, A.10, A.11) that the average effective twist of individual ribbons in the fibril for $\tilde{k}\ll 1$ is nearly equal to γ_0.

$$\frac{\gamma_0-\gamma}{\gamma_0}\simeq-\left(\frac{25\tilde{\sigma}^2}{768}\right)^{1/5}\quad\text{in regime 2}\tag{A.17}$$

which is valid if

$$\tilde{\sigma}\ll\frac{16}{45}\tag{A.18}$$

$$\tilde{\sigma}\gg\frac{5}{8}\left(\frac{15}{2}\tilde{k}^5\right)^{1/2}.\tag{A.19}$$

The two conditions above (specifying regime 2, see Fig. 6) are equivalent to the condition (A.1) and to the condition that $\tilde{k}$ is subdominant in the r.h.s. of equation (A.7). Note that $\gamma\simeq\gamma_0$ since $\tilde{\sigma}\ll 16\sqrt{3}/5$ which follows from inequality (A.18).

In regime 2 the fibrils are stable ($\mathcal{E}<0$, $p\geq 2$) if

$$\tilde{\sigma}\gtrsim\frac{16}{45}\left(\gamma_0 a\right)^5\quad\text{in regime 2}\tag{A.20}$$

(see Eqs. (10, A.2, A.16, A.17, A.19). Note that in regime 2 the parameter $\tilde{k}$ drops out of the resulting equations (A.16, A.17, A.20).

A.3 Regime 3: strongly untwisted thin fibrils

One can easily understand that the situation opposite to the one considered above (in regimes 1 and 2: $\gamma\simeq\gamma_0$) is when $\gamma\ll\gamma_0$ (we still consider the case of thin fibrils, see condition (A.1)). From equations (A.3, A.4) we get $\tilde{k}(\gamma/\gamma_0)\simeq 6/(ap\gamma)^2\gg 1$, and finally

$$\gamma\simeq\gamma_0\frac{3}{2\tilde{k}\tilde{\sigma}^2}\tag{A.21}$$

$$ap\gamma_0\simeq\frac{4\tilde{k}\tilde{\sigma}^3}{3}\qquad\text{in regime 3.}\tag{A.22}$$

This situation is realized if the following conditions are satisfied:

$$\tilde{\sigma}\ll 1\tag{A.23}$$

$$\tilde{\sigma}\gg\left(\frac{3}{2\tilde{k}}\right)^{1/2}\tag{A.24}$$

which follow from equation (A.1) and the condition $\gamma\ll\gamma_0$. This regime is indicated as *regime* 3 ('strongly untwisted thin fibrils') in the diagram of Figure 6.

The fibril is stable ($\mathcal{E}<0$, $p\geq 2$) provided that (see Eqs. (10, A.2, A.21, A.22))

$$\tilde{\sigma}\gtrsim\frac{1}{2}\gamma_0 a\quad\text{in regime 3.}\tag{A.25}$$

Note that from the conditions (A.24, A.25) it follows that $p\gg 1$ as it is required for our consideration (cp. Eq. (A.15)).

Appendix B: The asymptotic case of thick sheet-like fibrils (large β)

B.1 Regime 4: wide sheets

The limit opposite to that of (A.1) is when the stack formed by ribbons is very wide:

$$\beta\gg 1.\tag{B.1}$$

Under this condition the functions (12, 15) can be approximated as

$$C\simeq\frac{\pi}{2};\quad D\simeq 0;\quad C'\simeq\frac{1}{\beta^2};\quad D'\simeq-\frac{1}{\beta^2},\tag{B.2}$$

and hence the system of equations (13, 14) has the following solution:

$$\beta\simeq\frac{4}{(\pi-\tilde{\sigma})};\quad\beta_0\simeq\frac{2\pi\left(1+\tilde{k}\right)}{(\pi-\tilde{\sigma})^2}\tag{B.3}$$

i.e.

$$\gamma\simeq\gamma_0\frac{2\left(\pi-\tilde{\sigma}\right)}{\pi\left(1+\tilde{k}\right)};\quad p\simeq\frac{1}{a\gamma_0}\frac{2\pi\left(1+\tilde{k}\right)}{(\pi-\tilde{\sigma})^2}.\tag{B.4}$$

The following inequalities should be fulfilled in order to satisfy the condition (B.1)

$$0<\pi-\tilde{\sigma}\ll 1\tag{B.5}$$

which define *regime* 4 ('wide sheets') in the diagram of Figure 6. These conditions ensure that $\gamma\ll\gamma_0$ and $pa\gamma\gg 1$, *i.e.* the stack (fibril) is strongly untwisted and it is very wide (but finite) even when compared to its twist period h (which is much longer than the primary one, h_0). Note also that $p\gg 1$ as $a\lesssim h_0$.

Wide fibrils (condition B.1) are stable ($\mathcal{E}<0$) if (see Eqs. (10, B.3))

$$\frac{\tilde{\sigma}}{\gamma_0 a}\gtrsim\frac{1}{2}-\frac{(\pi-\tilde{\sigma})}{4\beta_0}\tag{B.6}$$

Note that the last term in equation (B.6) is small in accordance with equations (B.3, B.5), hence this condition is in fact very close to (A.25).

B.2 Regime 5: infinite sheets

When $\tilde{\sigma}$, equation (11), approaches π from below, the equilibrium sheet-like fibril thickness tends to infinity, simultaneously the fibril looses its twist:

$$p\to\infty;\quad\gamma\to 0;\quad\beta\to\infty;\quad\beta_0/\beta\to\infty\tag{B.7}$$

see equation (B.4). Finite fibrils are replaced by infinite untwisted sheets if $\tilde{\sigma}\geq\pi$, *i.e.* if

$$\frac{\sigma ab}{\gamma_0 k_{\text{twist}}}\geq\pi\tag{B.8}$$

(regime 5 of Fig. 6). The stability condition is now exactly

$$\frac{\tilde{\sigma}}{\gamma_0 a} > \frac{1}{2}\,. \tag{B.9}$$

Note that in regime 5 the term in the curly brackets in equation (10) is tending to zero.

References

1. C. Branden, J. Tooze, *Introduction to protein structure* (Garland Publ.: N.Y. and London, 1991).
2. T.E. Creighton, *Proteins. Structures and molecular properties* (W.H. Freeman and Co: N.Y., 1993).
3. A. Aggeli, M. Bell, N. Boden, J.N. Keen, T.C.B. McLeish, I. Nyrkova, S.E. Radford, A. Semenov, J. Mater. Chem. **7**, 1135 (1997).
4. A. Aggeli, M. Bell, N. Boden *et al.*, Nature **386**, 259 (1997).
5. A. Aggeli *et al.*, Proc. Natl. Acad. Sci. USA, 2000 (submitted).
6. I.A. Nyrkova, A.N. Semenov, A. Aggeli, M. Bell, N. Boden, T.C.B. McLeish, Eur. Phys. J. B **17**, 499 (2000).
7. J.F. Marko, E.D. Siggia, Macromolecules **27**, 981 (1994).
8. J.F. Marko, E.D. Siggia, Science **265**, 506 (1994).
9. G.E. Arnold, L.A. Day, A.K. Dunker, Biochemistry **31**, 7948 (1992).
10. I.B. Grishina, R.W. Woody, Faraday Discuss. **99**, 245 (1994).
11. I.A. Bolotina, V.Y. Lugauskas, Molecular Biol. **19**, 1154 (1985).
12. A.Yu. Grosberg, A.R. Khokhlov, *Statistical Physics of Macromolecules* (New York: AIP Press, 1994).
13. J.N. Israelachvili. *Intermolecular and Surface Forces. With Applications to Colloidal and Biological Systems* (Academic Press Inc. (London) Ltd., 1985).
14. I.A. Nyrkova, A.N. Semenov, J.-F. Joanny, J. Phys. II France **7**, 847 (1997).
15. S.Y. Tan, M.B. Pepys, Histopathology **25**, 403 (1994).
16. M. Sunde, C.C.F. Blake, Quarterly Rev. Biophys. **31**, 1 (1998).
17. P.E. Fraser, J.T. Nguyen, W.K. Surewicz, D.A. Kirschner, Biophys. J. **60**, 1190 (1991).
18. Y. Shen, M.A. Johnson, D.C. Martin, Macromolecules **31**, 8857 (1998).
19. M. Osumi, Micron **29**, 207 (1998).
20. E. Scherzinger *et al.*, Proc. Natl. Acad. Sci. USA **96**, 4604 (1999).
21. M.J. Burke, M.A. Rougvie, Biochemistry **11**, 2435 (1972).
22. W.B. Gratzer, G.H. Beaven, H.W.E. Rattle, E.M. Bradbury, Eur. J. Biochem. **3**, 276 (1968).
23. H.H. Bauer, U. Aebi, M. Hauner *et al.*, J. Structural Biol. **115**, 1 (1995).
24. J.-F. Revol, H. Bradford, J. Giasson, R.H. Marchessault, D.G. Gray, Int. J. Biol. Macromol. **14**, 170 (1992).
25. J. Lydon, in *Handbook of Liquid Crystals, v.2*, edited by D. Demus, J. Goodby, G.W. Gray, H.-W. Spiess, V. Vill, 981 (Wiley-VCH: Weinheim, N.Y., Chichester, Brisbane, Singapore, Toronto, 1998)
26. E.E. Jelley, Nature **138**, 1009 (1936); *ibid* **139**, 631-632 (1937).
27. W.J. Harrison, D.L. Mateer, G.J.T. Tiddy, J. Phys. Chem. **100**, 2310 (1996).
28. T. Gotoh, T. Nakata, G. Saitoh, M. Satoh, E. Hasegawa, NEC Res. & Dev. **38**, 394 (1997).
29. W.A. Eaton, J. Hofrichter, in *Advances in Protein Chemistry*, (Academic Press, Inc.: San Diego, pp. 63, 1990).
30. M.S. Spector, *et al.*, Langmuir **14**, 3493 (1999).
31. R. Oda, I. Huc, S. Candau, F.C. MacKintosh, Nature **399**, 566 (1999).
32. A. Kitamura, T. Kiyota, M. Tomohiro *et al.*, Biophysical J. **76**, 1457 (1999).
33. T. Gulik-Krzywicki, C. Fouquey, J.M. Lehn, Proc. Natl. Acad. Sci. USA **90**, 163 (1993).
34. A.E. Rowan, R.J.M. Nolte, Angew. Chem. Int. Ed. **37**, 63 (1998).
35. P. Terech, R.G. Weiss, Chem. Rev. **97**, 3133 (1997).
36. K. Murata, M. Aoki, T. Suzuku, T. Harada, H. Kawabata, J. Am. Chem. Soc. **116**, 6664 (1994).
37. J.-H. Fuhrhop, W. Helfrich, Chem. Rev. **93**, 1565 (1993).
38. K. Hanabusa, M. Yamada, M. Kimura, H. Shirai, Angew. Chem. Int. Ed. **35**, 1949 (1996).
39. K. Akagi, G. Piao, S. Kaneko *et al.*, Science **282**, 1683 (1998).